Applied Energy 283 (2021) 116239

Contents lists available at ScienceDirect

Applied Energy

journal homepage: www.elsevier.com/locate/apenergy

Extensive comparison of physical models for photovoltaic power forecasting

Martin János Mayer [a,b,*], Gyula Gróf [a]

[a] Department of Energy Engineering, Faculty of Mechanical Engineering, Budapest University of Technology and Economics, Műegyetem rkp. 3, Budapest 1111, Hungary
[b] MVM Hungarian Electricity Ltd., Szentendrei út 207, Budapest 1031, Hungary

HIGHLIGHTS

- Irradiance separation and transposition modeling are the two most critical steps.
- 13% MAE, 12% RMSE and 23–33% skill score improvement is possible by model selection.
- Detailed physical model chains, inlc. reflection and shading, have the lowest MAE.
- Simple models have the lowest RMSE, but high bias and underdispersed forecast.
- Wind speed has only marginal effect on physical photovoltaic power forecasting.

GRAPHICAL ABSTRACT

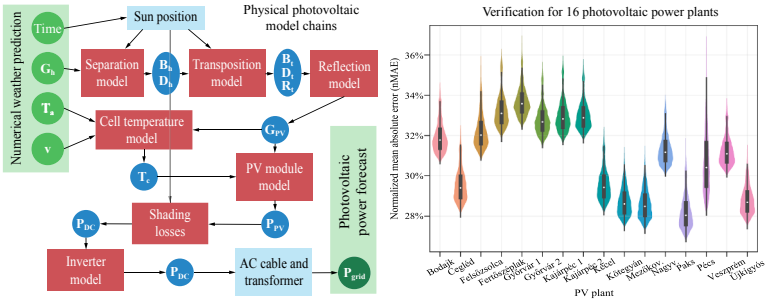

ARTICLE INFO

Keywords:
Photovoltaic forecast
Power prediction
Grid-connected photovoltaic plants
Physical approach
PV simulation

ABSTRACT

Forecasting the power production of grid-connected photovoltaic (PV) power plants is essential for both the profitability and the prospects of the technology. Physically inspired modelling represents a common approach in calculating the expected power output from numerical weather prediction data. The model selection has a high effect on physical PV power forecasting accuracy, as the difference between the most and least accurate model chains is 13% in mean absolute error (MAE), 12% in root mean square error (RMSE), and 23–33% in skill scores for a PV plant on average. The power forecast performance analysis performed and verified for one-year 15-min resolution production data of 16 PV plants in Hungary for day-ahead and intraday time horizons on all possible combinations of nine direct and diffuse irradiance separation, ten tilted irradiance transposition, three reflection loss, five cell temperature, four PV module performance, two shading loss, and three inverter models.

The two most critical calculation steps are identified as irradiance separation and transposition modelling, while the inverter models are the least important. Absolute and squared errors are two conflicting metrics, as the more detailed models result in the lowest MAE, while the simplest ones have the lowest RMSE. Wind speed forecasts have only a marginal effect on the PV power prediction. The results of this study contribute to a deeper understanding of the physical forecasting approach in the research community, while the main conclusions are also beneficial for PV plant owners in preparing their generation forecasts.

Abbreviations: AROME, Application of Research to Operations at Mesoscale; ANN, artificial neural network; CMV, cloud motion vector; DA, day-ahead (24–48 h); ECMWF, European Centre for Medium-Range Forecasts; GHI, global horizontal irradiance; ID, intraday (0–24 h); NWP, numerical weather prediction; PV, photovoltaic; RF, random forest; STC, standard test conditions; SVM, support vector machine.

* Corresponding author at: Department of Energy Engineering, Faculty of Mechanical Engineering, Budapest University of Technology, Műegyetem rkp. 3, Budapest 1111, Hungary.
E-mail address: mayer@energia.bme.hu (M.J. Mayer).

https://doi.org/10.1016/j.apenergy.2020.116239
Received 24 July 2020; Received in revised form 20 October 2020; Accepted 1 November 2020
Available online 4 December 2020

Nomenclature

Greek letters

Θ_Z	solar zenith angle, °

Latin letters

AM	air mass
B	beam irradiance, W m^{-2}
D	diffuse irradiance, W m^{-2}
F	variance ratio
G	global irradiance, W m^{-2}
k_D	diffuse fraction
k_N	atmospheric transmittance
k_T	clearness index
P	power, W
MAE	mean absolute error
MBE	mean bias error
MSE	mean square error
RMSE	root mean square error
s	skill score
t_s	apparent solar time
v	wind speed, m/s
$\mathbb{V}$	variance
W	precipitable water, cm
Y	annual specific energy yield, kWh/kW

Suffixes

a	ambient
AC	alternating current
cp	optimal climatology-persistence reference forecast
cs	clear sky
DC	direct current
fc	forecasted data
h	horizontal
meas	measured data
mean	average value
NOCT	nominal operating cell temperature
p	persistence reference forecast
PV	photovoltaic module
ref	reference

1. Introduction

Photovoltaic (PV) systems became the fastest-growing renewable technology in the last decade [1]. Due to the intermittent nature of the solar irradiance, accurate forecasting techniques are essential for the effective grid integration of the PV plants [2]. Accordingly, with an exponentially growing number of published papers, solar forecasting emerged as one of the most prevalent areas of renewable energy research [3]. The term "solar forecasting" is used in two senses; it stands for both solar irradiance and solar (mostly photovoltaic) power forecasting [4]. The PV power predictions are either calculated from irradiance forecast data, produced by sky or satellite imagery or numerical weather prediction (NWP), or forecasted directly from a range of possible predictors [5]. The power calculation methods are classified into three main categories, *physical*, *statistical*, and *hybrid* approaches [6]. The *physical* methods use a theoretical simulation model to calculate the output power of a PV system based on its main design parameters. The *statistical* term, in this context, includes all data-driven methods, covering both the classical statistical modelling and the novel machine learning algorithms. The *hybrid* method is a combination of two different methods, either a physical and a statistical, or two or more statistical models [5].

The literature suggests that statistical methods are most commonly used for PV power forecasting [7]. These data-driven methods are based on historical irradiance and production datasets, and they do not require any information regarding the design parameters of the PV system. Li et al. [8] presented a successful application of multivariate adaptive regression splines for daily PV output forecasting. Leva et al. [9] used an artificial neural network (ANN) to calculate day-ahead PV output power from weather forecast data. Wang et al. [10] compared deep learning models, including convolutional neural networks, long-short term memory network, and their combination for day-ahead PV forecasting from meteorological data. Theocharides et al. [11] analyzed the application of artificial neural networks and the effect of statistical post-processing for day-ahead PV production forecasting based on NWP data. Antonanzas et al. [12] used Support Vector Machine (SVM) and Random Forest (RF) machine learning techniques for NWP-based day-ahead PV power forecasting and analyzed the market value provided by the forecast. Among these examples, many other studies demonstrate the effectiveness of different machine learning methods for day-ahead PV power forecasting based on radiation forecasts [13]. However, the accuracy of the data-driven forecasts largely depends on the length of the training dataset, and the accuracy of even the most novel deep learning methods is limited if only less than 1–3 years of historical data is available [10].

The physical power calculation approach is based only on the main design parameters of the PV system, and it does not require any historical data. Therefore, it is a useful way for PV plant owners who have all the necessary information available in the design documentation of the plant. Regarding its accuracy, evidence can be found for both lower [14] and higher [15] performance of the physical modelling compared to machine learning methods. However, most studies agree that hybrid models, e.g., by adding physically-calculated properties [16] or even just the clear sky irradiance [17] to the inputs of a neural network, overperform either the purely physical or statistical approach. Physical PV power forecasting models have a high significance in two main applications, in 1) power prediction of new PV installations where no historical production data is available, and 2) hybrid physical and data-driven modelling, which is the most accurate PV power forecasting technique [16].

The physical modelling of PV power output from irradiance forecast data requires a *model chain* consisting of several calculation steps. Yang et al. [18] identified the three main steps as the separation of the beam and diffuse irradiance, the transposition of horizontal irradiance to the tilted surface, and the PV performance modelling. Lorenz et al. [19] used a physical model including four calculation steps for the day-ahead hourly regional prediction of the German PV production based on the forecasts of the global model of the European Centre for Medium-Range Forecasts (ECMWF). The four steps are the irradiance transposition (Perez), cell temperature (linear), PV performance (Beyer), and inverter (quadratic) models. (Small caps are used thorough this paper for the name of models.) Wolff et al. [15] compared support vector regression (SVR) with physical modelling for power forecasting based on a satellite-derived cloud motion vector (CMV) and NWP irradiance forecasts. The physical PV simulation is constructed from five steps, namely the Skartveit-Olseth separation and the Klucher transposition, the linear temperature, the Beyer PV performance, and the quadratic inverter models. Results show that the physical models enhanced by a simple linear regression overperformed the SVR, especially based on the NWP irradiance data. Saint-Drenan et al. [20] proposed a method for estimating the main parameters of a PV system from historical production and irradiance forecast data using a physical PV model. In addition to the calculation steps mentioned above, this model also includes the Martin-Ruiz angular loss model to account for the reflection losses from

the module surface. Holland et al. [21] applied a physical model, consisting of the DIRINT separation, Perez transposition, and an in-house PV performance simulation models, to forecast PV power from NWP and local irradiance measurement data. Amaro e Silva and Brito [22] used physical modelling, including the Engerer separation, Perez transposition, and Martin-Ruiz angular loss model for spatio-temporal very short-term forecasting of PV power based on the production of neighbouring PV systems. Almeida et al. [14] compared a detailed physical model with nonparametric Quantile Regression Forests for hourly day-ahead forecasting of 6 PV systems. The physical model chain includes the Erbs separation, Perez transposition, Martin-Ruiz angular loss, Faiman temperature, Evans PV, and quadratic inverter model, and also considers the shading, spectral, and inverter losses. A comparison with local irradiance and temperature measurements shows that in cloudy weather, most of the power forecast error comes from the irradiance forecast. In contrast, under clear sky conditions, when the meteorological forecast is quite accurate, the physical model is the main source of error.

Even though the best models of the main calculation steps are known for research-grade data from worldwide comparisons, but these overall best models are not always the most accurate for imperfect input data [23], such as the inherently erroneous irradiance forecasts. However, in most of the above-presented studies, the physical model selection is rather arbitrary, and neither a comparison of different model chains nor an evaluation of the effect of model selection on the forecast error is presented. Only two papers are known to the authors to include such a comparison. Pelland et al. [24] presented an hourly day-ahead power forecasting for three Canadian PV system based on the Global Environmental Multiscale NWP forecast model. The physical power calculation model was selected as the best possible combination of three separation models (Orgill-Hollands, Reindl, Erbs), four transposition models (Liu-Jordan, Hay-Davies, Perez, Reindl) and two PV (linear, PVSAT) models, but their differences are not discussed in detail. Dolara et al. [25] compared three PV (single diode with 3, 4, and 5 parameters) and two cell temperature (NOCT, Sandia) models using measured weather and power data. The irradiance on the PV modules is calculated by the Liu-Jordan transposition and Martin-Ruiz angular loss model, but their effect and selection are not examined. The results show that the simpler models often overperform the more complex ones. No study has been prepared yet that presented the effect of the model selection in all steps of the physical modelling chain.

Despite the importance of physical irradiance-to-power calculation methods, no answers can be found in the literature to such relevant questions as 1) how the selection of the physical models influences the power forecast accuracy, 2) what are the most accuracy-critical modelling steps, and 3) which model chain should be chosen for an operational PV forecasting? This paper aims to fill this gap by an extensive comparison and verification of different physical PV forecasting methods for intraday and day-ahead time horizons based on NWP data with 15 min resolution. A general schematic of a physical model chain consisting of seven main calculation steps is proposed, and multiple models are selected for comparison in all of these main steps. Nine direct and diffuse irradiance separation, ten tilted irradiance transposition, three reflection loss, five cell temperature, four PV performance, two shading loss, and three inverter models are included in the comparison. All possible combinations of these models result in 32,400 different model chains, which are verified for the deterministic 16 power plants for both 24-h and 48-h time horizons based on one-year-long production and NWP datasets. The conclusions derived from the comprehensive analysis of the results contribute to a deeper understanding of the physical modelling process and facilitates the practical application of the physical PV forecasting methods.

The concept of the physical model chain and a summary of the applied models is introduced in Section 2. The verification framework, including all relevant information about the data and performance metrics, is described in Section 3. The comparison of the models and the evaluation and discussion of the results are presented in Section 4. Conclusions are drawn, and further research areas are proposed in Section 5.

2. Photovoltaic plant performance model variants

The general concept of the detailed performance modelling of PV systems is visualized in Fig. 1. This approach identifies the following seven main modelling steps: (i) separation of the global horizontal irradiance (GHI) into the beam and diffuse components, (ii) transposition of the horizontal irradiance to the tilted plane of the PV array, (iii) calculation of the reflection losses, (iv) calculation of the cell temperature, (v) calculation of the PV module efficiency, (vi) estimation of the shading losses, (vii) calculation of the inverter losses. These main steps are supplemented by the calculation of the position of the Sun and the estimation of other less significant system losses. In this study, this general framework is used for the modelling of ground-mounted PV power plants, but with some minor modifications, it can also be applied to any other types of PV systems [26]. This modeling concept is widely used not only in forecasting but also in PV design optimization applications [105].

The inputs are the numerical weather prediction (NWP) data with GHI, ambient temperature, and wind speed values for each timestamp, while the output is the power generated by the PV plant. If the wind speed is not available in the NWP data, the model can still be used with only a minor decrease in the accuracy as wind speed has only a slight influence on the PV production (see Section 4.6) [27]. In case not only the GHI but both its beam and diffuse components are provided in the NWP dataset, the separation model can be skipped, and the calculation can be started with the transposition model.

There are no exact methods to determine the outputs with perfect accuracy in any of the modelling steps, but tens or even hundreds of different model variants can be found in the literature for each of the main steps. The featured models are selected according to two criteria: simplicity and accuracy. First, the simplest models are chosen for each step to serve as a baseline in comparison with the more elaborated ones. Besides, the models that performed among the bests in review papers and are well-known and widely used in the research community are also included. The full lists of the selected models are summarized in tabular form in the next subsections. These models are not described in detail due to their large number, but references are given to the original publications where the readers can find their full description and explanation. However, all relevant details regarding the implementation and parametrization of these models are specified here to ensure the reproducibility of the calculations. The modelling steps are independent, so all possible combinations of the nine separation, ten transposition, three reflection loss, five cell temperature, four PV module power, two shading loss, and three inverter models are valid and complete PV plant model chains, which results in 32,400 possible model formulations.

The position of the Sun, represented by the solar zenith and azimuth angles, is calculated by the solar position algorithm described in [28] using the *pvlib* python package [29].

2.1. Beam and diffuse separation models

The separation (or decomposition) models are used to estimate the B_h beam and D_h diffuse components of the global horizontal irradiance. Most of these models estimate the k_D diffuse fraction (defined as the ratio of the diffuse to the global horizontal irradiance) as a function of the k_T clearness index (the ratio of the GHI to its extraterrestrial counterpart) and other predictors. The other models were created to determine the direct normal irradiance (DNI), and they give an expression for the k_N atmospheric transmittance (the ratio of the DNI and the extraterrestrial irradiance) using a similar set of predictors. These models can also be used for the diffuse fraction calculation through the closure equation:

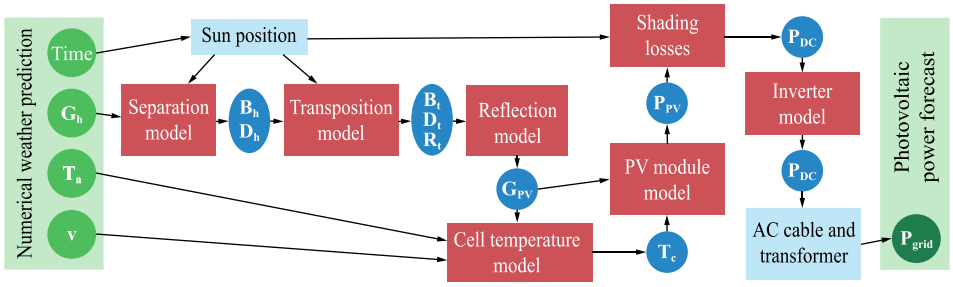

Fig. 1. Concept of the physical PV power plant performance modelling based on NWP data. Red boxes represent the seven main modelling steps where multiple model variants are compared in this study.

$$k_D = 1 - k_N/k_T \quad (1)$$

The most comprehensive review and validation of the separation models were presented by Gueymard and Ruiz-Arias [30], who compared 140 separation models for five climatic regions. An essential trait of these models is the number of predictor variables: more than half of them use k_T as the single predictor, while the more complex models are based on even 5 or 6 different variables. The models presented here only use such predictors that can be calculated from the time and the GHI, as only these two data are generally available in the NWP forecast. A more recent model proposed by Yang and Boland [31], even though it is claimed to be the best separation by now [32], is omitted here as it requires a satellite-derived diffuse fraction as a predictor, which is not available from NWP forecasts.

This study compares the nine separation models listed in Table 1. The Erbs model was chosen due to its simplicity. The next six due to their good performance in the referenced validation study [30], and the last two due to their novelty.

2.2. Tilted irradiance transposition models

Transposition models are used to estimate the irradiance on a tilted surface with arbitrary orientation based on the beam and diffuse horizontal irradiance. The G_t global tilted irradiance is the sum of a beam, a diffuse, and a ground-reflected component. The transposition of the beam irradiance is purely geometrical and based on the cosine of the incidence angle and the zenith angle. The ground-reflected irradiance is considered isotropic in most studies and calculated from the GHI with the ground albedo and an isotropic transposition factor [46]. A ground albedo of 0.2 is assumed in this study for all locations [23].

The difference between the transposition models is the treatment of diffuse irradiance. The simple Liu-Jordan model assumes an isotropic diffuse irradiance over the whole sky globe and calculates the diffuse transposition factor as a view factor between the modules and the sky. The more complex models also consider a circumsolar or even a horizontal brightening diffuse components. The most comprehensive review and benchmark of transposition models by now was presented by Yang [46], which identified the Perez model as the overall best performer.

The ten transposition models compared in this study are summarized in Table 2. The Liu-Jordan model is included due to its simplicity, the Kulcher due to its popularity [6,15], and the others due to their above-average benchmark performance in [46].

Table 1
List of the compared beam and diffuse irradiance separation models.

Nr.	Name	Reference	Predictors	Comment
1	Erbs	Erbs et al. (1982) [33]	k_T	
2	Skartveit	Skartveit and Olseth (1987) [34]	k_T, Θ_Z	
3	DISC	Maxwell (1987) [35]	k_T, AM	AM is calculated by the Kasten and Young [36] formula
4	DIRINT	Perez et al. (1992) [37]	k_T', Θ_Z, W, $\Delta k_T'$	The model is used with the universal bin for W as the exact value if not available
5	DIRINDEX	Perez et al. (2002) [38]	k_T', Θ_Z, W, $\Delta k_T'$, $G_{h,cs}$, DNI_{cs}	Paired with the Ineichen-Perez clear sky model [39], and W is treated similarly as for DIRINT
6	BRL	Ridley et al. (2010) [40]	k_T, Θ_Z, t_s, K_T, ψ	
7	Engerer	Engerer (2015) [41]	k_T, Θ_Z, t_s, $\Delta k_{T,cs}$, K_{de}	Paired with the Threlkel-Jordan clear sky model [42], and used with the 15 min parametrization presented in [43]
8	Starke	Starke et al. (2018) [44]	k_T, Θ_Z, t_s, K_T, ψ, $G_{h,cs}$	Paired with the Ineichen-Perez clear sky model [39], and used with the parametrization for Brazil
9	Abreu	Abreu et al. (2019) [45]	k_T	Used with the parametrization for the temperate climate zone

2.3. Reflection loss model

The reflection from the module surface and the increased absorption in the module cover both depend on the incidence angle of the incoming radiation. These losses are called angular losses, and they can be estimated as a function of the incidence angle. They can be calculated by a physical model, which describes the reflectivity of the air-glass interface

Table 2
List of the compared diffuse irradiance transposition models.

Nr.	Name	Reference	Comp.	Comment
1	Liu-Jordan	Liu-Jordan (1961) [47]	1	
2	Steven	Steven and Unsworth (1979) [48]	2	Following the way as it is implemented in [46] under the Steven4 name
3	Hay	Hay and Davies (1980) [49]	2	
4	Willmot	Willmot (1982) [50]	2	
5	Skartveit	Skartveit and Olseth (1986) [51]	2	
6	Gueymard	Gueymard (1987) [52]	2	Considering the Erratum [53]
7	Muneer	Muneer (1990) [54]	2	Sky-diffuse irradiance parameters for Geneva [54], and the overcast condition is defined as $k_T' < 0.3$ as proposed in [55]
8	Klucher	Klucher (1979) [56]	3	
9	Perez	Perez et al. (1988) [57]	3	Used with the parametrization presented in Table 6 of [58]
10	Reindl	Reindl et al. (1990) [59]	3	

with Snell's and Fresnel's law [60]. These losses can also be estimated by empirical formulations, like the ASHRAE [61], Martin-Ruiz [62], and the Sandia [63] models, but despite their different mathematical equation, they all result in a similar curve when the loss factor is plotted against the angle of incidence. Thus, their accuracy can not be substantially different, so only the Martin-Ruiz empirical formula is implemented in this study. As the simplest alternative, these losses can be neglected, as this calculation step is not an essential part of the whole modelling process, and it is also omitted from many physical forecasting studies [6,15,21]. The three compared reflection loss calculation methods are listed in Table 3.

2.4. Cell temperature models

The cell temperature models estimate the temperature of the PV cell, which has a significant effect on the electrical characteristics and efficiency of the PV modules. The cell temperature mainly depends on the ambient temperature and the absorbed irradiance, and some models also consider the cooling effect of the wind [65]. Since the converted part of the absorbed radiation does not contribute to the heating of the module, the electrical efficiency also influences the cell temperature [66]. Thus, higher efficiency results in lower cell temperature, which is taken into account in the Mattei and Skoplaki models. The latest review of the topic presents 20 cell temperature models, where most of them are only a different parametrization of the five mathematical formulations included in this study [65]. The v_m wind speed at the height of the modules is calculated using the power law with an exponent of 0.25 [67].

The five cell temperature models compared in this study are listed in Table 4. The NOCT model is one of the simplest cell temperature models, while others are selected due to their popularity and good performance in comparative studies [68].

2.5. Photovoltaic module performance models

The PV module performance models describe the effect of the cell temperature and irradiance on the efficiency of a PV module. The spectrum of the radiation also influences the efficiency, which can be considered by a spectral mismatch factor calculated from the spectral response of the cells and the spectrally-resolved radiation data [73]. In the case only the broadband irradiance is available without any spectral information, the spectral effects can only be estimated, e.g., as a function of the air mass as proposed in [63]. However, this simple correlation does not account for the significant effect of the cloud cover [74]. As the spectral mismatch of crystalline silicon modules is the lowest among the different PV technologies [73,75], this effect is neglected in this study.

The PV performance models can be classified into two categories: empirical models, that calculate the MPP power as a function of the cell temperature and irradiance using an empirical equation, and physical models, that are based on the single or two-diode equivalent circuit of the PV cells [76]. A detailed review of the physical modelling of PV modules, including the different module formulations and parameter estimation techniques, can be found in [77]. Both the number of model parameters and the parameter estimation method influence the accuracy of the single-diode PV models [25].

The four PV performance models compared in this study are listed in Table 5. The Evans model is the simplest empirical PV model, which only takes the effect of cell temperature into account, while the Huld model is a more elaborated empirical one. The single diode 4 and single diode 5 are, respectively, the 4-parameters (shunt resistance neglected) and 5-parameters version of the single diode model, as proposed in [78].

Table 3
List of the compared reflection loss models.

Nr.	Name	Reference	Comment
1	None		
2	Martin-Ruiz	Martin and Ruiz (2001) [62]	Parameters for polycrystalline PV module
3	Physical	Marion (2017) [64]	Parameters for uncoated glass surface ($n = 1.526$)

Table 4
List of the compared cell temperature calculation models.

Nr.	Name	Reference	Predictors	Comment
1	NOCT	Ross (1982) [69]	G_{PV}, T_a	T_{NOCT} is taken from the datasheet of the module
2	King	King et al. (2004) [63]	G_{PV}, T_a, v_m	Parameters for glass/cell/glass module type and open rack mounting type are used
3	Faiman	Skartveit Faiman (2008) [70]	G_{PV}, T_a, v_m	$U_0 = 30.02$ and $U_1 = 6.28$ parametrization is used as proposed in [71]
4	Mattei	Mattei et al. (2006) [66]	G_{PV}, T_a, v_m	$U_{PV} = 26.6 + 2.3v_m$ and $\tau\alpha = 0.81$ parametrization is used
5	Skoplaki	Skoplaki et al. (2008) [72]	G_{PV}, T_a, v	Eq. (17) of [72] with $h_w = 26.6 + 2.3v$ convection coefficient and $\tau\alpha = 0.9$

2.6. Shading loss model

The uneven irradiance on the surface of the PV array can lead to significant power losses, which can be captured by a shading loss model. The shading losses with an intense stochastic nature, e.g., the effect of moving clouds [80], are not considered as they can not be quantified based on the NWP forecast data. Contrarily, the shading of the beam irradiance due to the adjacent mounting structure rows is deterministic, and the calculation of the shaded fraction of the modules is purely geometrical [81]. The power losses can be estimated considering the electric mismatch of the connected partially shaded cells, which can be done by either summing the IV characteristics of all cells or by a simplified approach [82]. A simplified method is adopted here due to its computational effectiveness and lower data requirements. The shading losses can also be neglected if no geometric information is available or the plant does not have a regular layout. The two shading loss calculation methods are listed in Table 6.

2.7. Inverter models

The inverter models calculate the losses of the inverters, considering the efficiency of the DC-AC conversion and the power and voltage limits of the inverter. The voltage limits are typically taken into account during the design process to keep the string MPP voltage within the limits of the inverter, thus, in well-designed PV plants, no voltage-related losses are expected during the operation. In terms of power, however, it is a common design practice to connect a higher DC power to the inverter than its nominal power. In this case, the output power is limited to the

Table 5
List of the compared photovoltaic module performance models.

Nr.	Name	Reference	Comment
1	Evans	Evans et al. (1977) [79]	β temperature coefficient is taken from the modules' datasheet
2	Huld	Huld et al. (2011) [75]	
3	Single diode 4	De Soto et al. (2006) [78]	Parameters estimated based on STC short-circuit, open-circuit and MPP I-V values from the datasheet and 96.5% relative efficiency at 200 W/m^2
4	Single diode 5	De Soto et al. (2006) [78]	Assumed $R_{sh,STC} = 400\ \Omega$, other parameters calculated in the same way as for the Single diode 4 model

Table 6
List of the compared shading models.

Nr.	Name	Reference	Comment
1	None		
2	Direct shading	Mayer and Gróf (2020) [83]	Direct shading calculation as presented in Section 3.2 of [83], without the diffuse shading effect

nominal power of the inverter, even if the MPP power of the modules is higher than its maximum input power [84]. These clipping losses are considered in all of the presented inverter models.

The inverter efficiency is commonly presented in the datasheet of the device in the form of three load-dependent efficiency curves at different input voltage levels, which needs to be translated to a mathematical formula. The simplest approach is to use a Constant average efficiency for all conditions. The Quadratic model fits a second-order polynomial as a function of input power to the nominal efficiency curve, while the Driesse model covers both the power and voltage dependence of the efficiency by a formula with nine parameters [85]. The three inverter efficiency models compared in this study are listed in Table 7.

2.8. Other losses

There are several other losses in PV plants that are not covered by the models of the seven main calculation steps. The main losses that are important to calculate in the plant design phase are described in [83]. The calculation of all these losses in forecasting application generally depends on which kind of relevant information is available for the PV plants of interest.

The cable losses are calculated based on the nominal voltage drop at design conditions, which is commonly specified in the design documentation of the plant. Effective cable resistance is calculated from the nominal current and voltage drop, while the actual voltage drop is calculated by multiplying the effective resistance with the actual current.

Regarding the other losses, two kinds of loss factors are specified in the design documentation of the studied PV plants: 1.68% for the transformer and medium-voltage components at nominal condition, and 0.64% for other electric losses, including the self-consumption and standby losses. The transformer loss factor is considered proportional to the output power, while the other is applied as a constant loss factor in all conditions. Due to the lack of relevant data, the losses due to soiling, stochastic shading effects, light-induced degradation, and module mismatch are not considered in this study.

3. Forecast verification framework

The physical model chain variants, covering all the 32,400 possible combinations (i.e., the Cartesian product) of the models described for each step in Section 2, are compared and verified for the operational deterministic power forecasting of 16 ground-mounted PV plants operating in Hungary on both intraday and day-ahead time horizons. This section summarizes all relevant information about the verification process: the description of the PV plants, the source of NWP data, the applied data quality control steps, the error metrics used for the forecasting performance evaluation, and an identification scheme for each model variants.

Table 7
List of the compared inverter efficiency models.

Nr.	Name	Reference	Predictors	Comment
1	Constant			European efficiency from the inverter datasheet
2	Quadratic	Driesse et al. (2008) [85]	P_{DC}	Eq. (1) of [85] fitted to the nominal efficiency curve from the inverter datasheet
3	Driesse	Driesse et al. (2008) [85]	P_{DC}, V_{DC}	Eq. (9) of [85] fitted to the efficiency curves at three voltage levels from the inverter datasheet

3.1. Photovoltaic power plants

The main parameters of the 16 ground-mounted, grid-connected PV plants are listed in Table 8. The plants are owned and operated by the MVM Green Generation Ltd, and all but one were commissioned in the second half of 2018 (the only exception is Pécs, which was installed in 2016). Győrvár 1 and 2, and Kajárpéc 1 and 2 are pairwisely located in the same village close to each other. The 14 individual plant locations are quite well distributed among the different parts of Hungary, as it is shown in Fig. 2. From a global point of view, they still cover quite a small area of the globe, and they all belong to the temperate climate zone. The expected annual energy production is around 1200 kWh/kW for most of Hungary; thus, the production data of Table 8 indicates that most of the examined PV plants produced well above the expectations in 2019.

3.2. Meteorological forecast data

The numerical weather prediction (NWP) data is provided by the Hungarian Meteorological Service from their operational AROME limited-area, high-resolution, non-hydrostatic, mesoscale weather forecast model. This model generates forecasts for 48 h time horizon with 15 min temporal and 2.5 km horizontal spatial resolution for a domain covering the Carpathian Basin. The global horizontal irradiance is calculated by the radiative transfer model of the ECMWF. A detailed overview of the model, including its parametrization and operational aspects, can be found in [86]. The verification of the GHI forecasts versus high-quality ground irradiance measurement is described in [87].

The NWP data used in this study are the (i) global horizontal irradiance, (ii) temperature at 2 m, (iii) wind speed at 10 m forecasts of the 00 UTC model run. The 48 h time horizon is ranging to the midnight of the next day and can be separated to a 0–24 h intraday (ID), and a 24–48 h day-ahead (DA) parts. The PV plant operators can utilize the DA part of each daily NWP to operators for creating the production schedule for the day-ahead market, while the ID part of the same forecast is suitable for a one-time bid refinement on the intraday market without any additional costs. The 15 min time resolution of the forecast is the same as the required resolution of the generation schedule; therefore, no interpolation or resampling is required during power calculation.

Table 8
Basic data of the 16 PV power plants used for the forecast model testing. P_{DC}: DC installed capacity, P_{AC}: AC nominal power, Y_{2019}: specific energy production for unit DC power in 2019.

Name	Coordinates	P_{DC} kW	P_{AC} kW	Y_{2019} kWh/kW
Bodajk	47.33° N, 18.22° E	590	498	1311
Cegléd	47.19° N, 19.80° E	590	498	1336
Felsőzsolca	48.12° N, 20.89° E	20,038	16,776	1262
Fertőszéplak	47.61° N, 16.84° E	590	498	1281
Győrvár 1	46.99° N, 16.83° E	590	498	1256
Győrvár 2	46.99° N, 16.83° E	590	498	1273
Kajárpéc 1	47.51° N, 17.62° E	590	498	1287
Kajárpéc 2	47.49° N, 17.62° E	590	498	1291
Kecel	46.53° N, 19.22° E	590	498	1337
Kötegyán	46.74° N, 21.48° E	590	498	1333
Mezőkovácsháza	46.40° N, 20.90° E	590	498	1355
Nagyvázsony	46.98° N, 17.69° E	590	498	1323
Paks	46.57° N, 18.82° E	20,680	17,244	1323
Pécs	46.06° N, 18.26° E	10,044	10,097	1211
Veszprém	47.10° N, 17.87° E	590	498	1324
Újkígyós	46.60° N, 20.99° E	590	498	1354

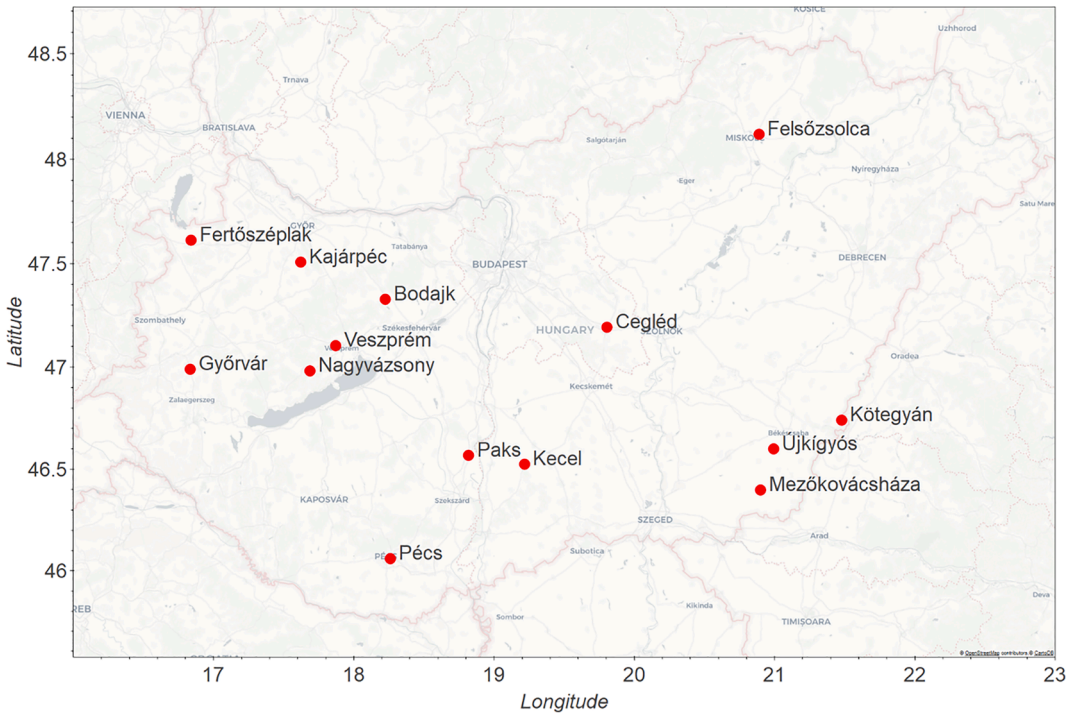

Fig. 2. Map of the photovoltaic power plant locations.

Regarding the accuracy of the NWP forecast, the Hungarian Meteorological Service provided an RMSE of 59 W/m^2 for Balatonberény (46.71° N, 17.31° E) and 53 W/m^2 for Nagykőrös (47.03° N, 19.78° E) for the whole 0–48 h time horizon. These values translate into a mean-normalized nRMSE of 41.0% and 37.4%, respectively.

3.3. Data quality control

The PV plant production data are retrieved from the official energy metering that is serving as a basis of the financial settlement and the imbalance calculation. The NWP data are coming from a reliable operational weather forecasting service with no missing or invalid data points. Accordingly, both datasets are of high quality, and no advanced quality control routine has to be performed to track any erroneous data [88].

The only applied quality control step is the exclusion of all daytime data entries when the power production of the plant is zero, as suggested in [27]. These zero values indicate the shutdown of the plant due to malfunctions or maintenances and appear only in 1.0–3.4% of the year, which is typical for PV plants in their first year of operation. The number of valid data points per plant is between 16,921 and 17517, and it is listed for all plants in Table 9.

A common practice in the radiation model validation [30] and forecast verification [32] studies is to exclude the data when the solar zenith angle is >85° due to the higher measurement and model errors and the limited energy production during this period. This approach is not adopted in this study as an operational PV forecast must provide a production schedule even for these early and late hours of the day; therefore, they cannot be just simply neglected in any practical applications. Nevertheless, the effect of this filter is marginal, as only 0.23–0.33% of the total annual energy was produced for >85° zenith angles.

Table 9
Average and variance of daytime power production and the performance of the naïve reference forecasts. The *p* suffix stands for persistence, while *cp* denotes the optimal combination of climatology and persistence.

Name	Valid data points	P_{mean} kW	$\mathbb{V}(P_{meas})$ kW^2	Intraday		Day-ahead	
				$nRMSE_p$	$nRMSE_{cp}$	$nRMSE_p$	$nRMSE_{cp}$
Bodajk	17,496	176.7	25,286	76.8%	69.4%	82.4%	73.3%
Cegléd	17,035	184.7	24,523	73.4%	66.2%	77.0%	68.6%
Felsőzsolca	17,300	5841.7	27,838,740	74.7%	68.0%	83.0%	73.7%
Fertőszéplak	17,499	172.6	25,457	81.7%	73.3%	87.3%	76.9%
Győrvár 1	17,467	169.4	24,585	84.0%	74.9%	88.3%	77.6%
Győrvár 2	17,452	171.9	25,134	82.1%	73.5%	86.6%	76.5%
Kajárpéc 1	17,339	175.1	25,182	80.1%	71.8%	86.0%	75.7%
Kajárpéc 2	17,371	175.3	25,021	80.6%	72.1%	86.6%	76.0%
Kecel	17,056	184.6	24,483	71.6%	64.9%	76.3%	68.1%
Kötegyán	16,921	185.5	24,794	68.0%	62.3%	73.1%	66.0%
Mezőkovácsháza	17,052	187.0	25,084	70.3%	63.9%	73.6%	66.3%
Nagyvázsony	17,513	178.0	25,633	79.9%	71.6%	84.4%	74.5%
Paks	17,179	6363.5	29,221,138	70.1%	63.9%	76.0%	67.9%
Pécs	16,993	2859.5	6,084,581	74.3%	67.1%	79.1%	70.3%
Veszprém	17,517	178.2	25,462	77.8%	70.1%	83.1%	73.6%
Újkígyós	17,061	186.9	25,206	69.4%	63.4%	73.5%	66.3%

3.4. Error and performance metrics

There is still no standardized method for the verification of photovoltaic power forecasts, but a recent paper authored by many prominent researchers of the solar forecasting field shows a forming consensus about the best evaluation method [32]. The main recommendations are the use of a distribution-oriented verification according to the Murphy-Winkler framework [89] and the root mean square error (RMSE) skill score as an indicator of the overall skillfulness of the forecast. Even though the joint distribution of the forecasts and measurements contains all time-independent information about the forecast performance, it is not suitable for the efficient comparison of the 32,400 different forecast results. Instead, the three most commonly used error metrics are calculated for the evaluation [4]:

- Mean absolute error (MAE):

$$MAE = \frac{1}{N}\sum_{i=1}^{N}\left|P_{fc} - P_{meas}\right| \tag{2}$$

- Mean bias error (MBE):

$$MBE = \frac{1}{N}\sum_{i=1}^{N}\left(P_{fc} - P_{meas}\right) \tag{3}$$

- Root mean square error (RMSE):

$$RMSE = \sqrt{\frac{1}{N}\sum_{i=1}^{N}\left(P_{fc} - P_{meas}\right)^2} \tag{4}$$

where P_{fc} and P_{meas} are the forecasted and measured power values, respectively, and N is the number of the valid daytime data entries. The nighttime values, as identified by a $>90°$ zenith angle, are excluded from the verification [32].

The electricity market structure, especially imbalance pricing (the penalty for schedule deviations) influences whether the RMSE or the MAE is the better indicator of the value of the forecast. RMSE penalizes the larger errors more heavily, which making it the most suitable indicator for the system operators as larger imbalances require the intervention of more costly reserves [6]. However, in most European markets, including Hungary, the PV plant owners have to pay imbalance penalties proportional to their forecast error, which is best described by the MAE [90]. Consequently, both error metrics are displayed in parallel in all evaluation steps.

The installed capacity and total energy production are different for all PV plants; therefore, all three error metrics are normalized to the mean power production. The P_{mean} average power values used for the nMAE, nMBE, and nRMSE calculations are listed in Table 9 for all PV plants. Even though recent studies recommend the use of the mean-normalized metrics [3,32], normalization to other quantities, like nominal or maximum power, is also common in the literature. As the daytime mean power is only around 28–32% of the installed DC capacity, the percentage value of a capacity-normalized metric is less than a third of the mean-normalized metrics presented in this study, which is important to consider during the comparison with other papers.

The variance of the forecast is a relevant indicator as it provides an insight into the spread and dispersion of the data [91]. For better comparability, the forecast variance can be normalized to the variance of the measured power of each plant:

$$F = \frac{\mathbb{v}(P_{fc})}{\mathbb{v}(P_{meas})} \tag{5}$$

where $\mathbb{v}(..)$ is the variance, and F is the variance ratio. $F > 1$ indicates the over-dispersion, while $F < 1$ is a sign of the underdispersion of the forecasted power compared to the actual measured values.

The skill score measures the forecast accuracy compared to a reference forecast based on a naïve forecasting method, calculated as the relative improvement of a chosen error metric [92]. The most widespread RMSE skill score is calculated as follows [32]:

$$s = 1 - \frac{RMSE_{fc}}{RMSE_{ref}} \tag{6}$$

The most commonly used naïve reference forecast is the persistence method, which assumes that the forecasted values over the whole time horizon remain the same as the last measurement [7]. In the case of day-ahead forecasting, the 24-h and 48-h persistence models are more appropriate benchmarks, as they use the measured power of the last available day as the forecast for the day of interest [93]. For a given day number d, the submitted intraday and day-ahead forecast applies for day d and $d+1$, respectively, while the last measured data are from day d-1. Accordingly, the 24-h persistence is the appropriate benchmark for the intraday, and the 48-h persistence is for the day-ahead part of the entire time horizon. Another well-accepted naïve forecast is climatology, which refers to the long-term average power of the plant [92]. Yang argues that the optimal convex combination of single-valued internal climatology and 24–48-h ahead persistence leads to the smallest RMSE among the naïve forecast methods; thus, this should be used as a standard reference for the skill score calculation [94]. This paper aims to follow both the common practice and the novel recommendations in order to ensure both the backward and forward comparability with other verification studies. Therefore, the skill scores are calculated for both the persistence (suffix p) and the optimal climatology-persistence (suffix cp) reference methods. The $nRMSE$ values of both reference forecasts are summarized in Table 9 for and all PV plants and time horizons.

3.5. Identification of physical model variants

The short but intuitive referencing of all the 32,400 different model variants is enabled by an alphanumeric code constructed from seven letters and each followed by a number. The letters stand for the modelling steps as follows:

- C: (component) separation model
- D: (diffuse) transposition model
- R: reflection model
- T: cell temperature model
- P: PV performance model
- S: shading model
- I: inverter model

The identification number after each letter is the number in the first column of Table 1–7. For example, C7D9R2T4P4S2I3 stands for the Engerer separation, Perez transposition, Martin-Ruiz reflection, Mattei cell temperature, 5-parameter single-diode PV performance, and Driesse inverter models, including the direct shading effect.

4. Results and discussion

The 32,400 different model chains are verified for all 16 PV plants and two time horizons, which results in 1,036,800 individual verification results, each calculated from around 17,000 valid daytime data points covering one year with 15 min resolution. There are many efficient methods for the performance evaluation of a single forecast or the comparison of several forecasts. However, no previous study is known in the context of PV forecasting that compared such a large number of individual forecast verification results. The evaluation is based on the

average performance of each component model, the range and distribution of the error metrics for each location, and the identification of the best performing model chains. Moreover, the methods and benefits of the optimal model selection and the effect of wind speed data is also assessed.

4.1. Average model performance

The averages of the six performance metrics are presented in Table 10 for each model, including all locations, time horizons, and model chains where the given model is used. All the values in Table 10 are an average of 103,680 (for transposition models) to 518,400 (for shading models) individual metrics. Therefore, even a small difference in these highly averaged values is significant, as a better value reflects that a given model generally performs better than the others regardless of the location, horizon, and the models used in the other steps of the model chains.

The highest differences in the average metrics can be seen by the separation and transposition models, which indicates that these are the two most critical calculation steps, i.e., the steps where the model selection has the highest impact on the overall forecast accuracy. On the other end, inverter modelling is the least critical, as there is only a very small difference between the three different models. The average bias is −0.3%, which indicates a slight underestimate of the power production, even though several unpredictable losses of the PV plants are not considered (see Section 2.8 for details). The average variance ratio of the forecasts is 91.9%, which indicates an average 8% underdispersion of the power forecasts. The transposition models have the highest effect on the variance ratio, as the Gueymard model ensures the highest variance, while the isotropic Liu-Jordan model leads to almost 17% underdispersion. In general, the simple models (like Liu-Jordan and NOCT, but even Hay and BRL) lead to lower, while the more detailed models (like Starke, Gueymard, Perez, DIRINDEX, Mattei, and Skoplaki) result in a higher variance. In the lack of measured irradiance data, it can not be

Table 10
Average error and performance metrics for all plants, time horizons, and model variants (better and worse than average values are indicated by green and red colours, respectively).

		nMAE	*nMBE*	*nRMSE*	s_p	s_{cp}	*F*
Separation	Erbs	29.5%	-1.1%	47.6%	39.2%	32.2%	90.9%
	Skartveit-Olseth	29.8%	-1.1%	47.8%	39.0%	31.9%	89.4%
	DISC	29.9%	0.5%	48.4%	38.3%	31.1%	92.0%
	DIRINT	29.7%	-0.1%	48.3%	38.3%	31.2%	92.3%
	DIRINDEX	30.6%	1.2%	49.2%	37.2%	29.9%	94.9%
	BRL	29.4%	-1.1%	47.4%	39.5%	32.5%	90.2%
	Engerer	29.7%	-2.0%	47.8%	39.1%	32.0%	89.4%
	Starke	29.5%	3.1%	48.5%	38.1%	30.9%	97.7%
	Abreu	29.6%	-2.0%	47.5%	39.4%	32.3%	89.9%
Transposition	Liu-Jordan	30.2%	-4.0%	47.2%	39.7%	32.7%	83.4%
	Steven	30.1%	3.1%	49.0%	37.5%	30.3%	95.4%
	Hay	29.7%	-0.9%	47.8%	39.0%	31.9%	90.3%
	Willmot	29.9%	-2.4%	48.0%	38.7%	31.6%	89.6%
	Skartveit-Olseth	29.7%	-1.2%	47.9%	38.9%	31.8%	90.5%
	Gueymard	29.7%	3.0%	49.1%	37.3%	30.0%	100.7%
	Muneer	29.5%	-2.1%	47.7%	39.1%	32.1%	91.4%
	Klucher	29.5%	0.8%	47.8%	39.0%	31.9%	92.2%
	Perez	29.6%	1.4%	48.2%	38.5%	31.3%	94.6%
	Reindl	29.7%	-0.6%	47.8%	39.0%	31.9%	90.7%
Refl.	None	29.9%	1.1%	48.2%	38.5%	31.3%	91.8%
	Martin-Ruiz	29.7%	-1.6%	48.0%	38.7%	31.6%	91.4%
	Physical	29.6%	-0.4%	47.9%	38.8%	31.7%	92.4%
Temperature	NOCT	30.0%	-2.1%	47.7%	39.2%	32.1%	87.1%
	King	29.9%	-1.4%	47.8%	39.0%	31.9%	89.1%
	Faiman	29.7%	0.1%	48.1%	38.6%	31.4%	92.9%
	Mattei	29.6%	0.9%	48.3%	38.4%	31.2%	94.8%
	Skoplaki	29.6%	1.1%	48.4%	38.3%	31.1%	95.4%
PV module	Evans	29.6%	1.5%	47.9%	38.8%	31.7%	92.2%
	Huld	29.9%	-1.8%	48.4%	38.3%	31.1%	94.5%
	Single diode 4	29.9%	-0.9%	47.9%	38.8%	31.7%	89.4%
	Single diode 5	29.7%	-0.1%	48.0%	38.8%	31.6%	91.4%
Shd.	None	30.0%	0.1%	48.2%	38.5%	31.3%	91.6%
	Beam shading	29.5%	-0.6%	47.9%	38.9%	31.8%	92.2%
Inverter	Constant	29.7%	-0.1%	48.0%	38.7%	31.6%	91.8%
	Quadratic	29.7%	-0.2%	48.1%	38.6%	31.5%	92.2%
	Driesse	29.8%	-0.6%	48.0%	38.7%	31.6%	91.6%
	Average	29.8%	-0.3%	48.1%	38.7%	31.5%	91.9%

determined whether the underdispersion originates from the NWP forecast or the physical power modelling introduce it.

In terms of the different performance metrics, the correlation between the MAE and RMSE is ambiguous: they well correlate among the separation, reflection and shading models, while their strong negative correlation can be observed among the transposition and cell temperature models. The BRL separation model has the lowest average errors in both absolute (MAE) and squared (RMSE) terms, and including the reflection and shading losses are also beneficial in both respects. In contrast, the Liu-Jordan transposition model has the lowest average RMSE and highest MAE at the same time. The skill scores are calculated from the RMSE; therefore, they entirely correlate, and the skill scores do not carry any additional information regarding the relative performance of the different models. The variance and the RMSE has a strong negative correlation, i.e., the more under-dispersed forecasts are better in terms of RMSE and forecast skill. This finding is consistent with the known tendency that spatial averaging improves the forecast performance [95].

4.2. Model chain accuracy range

The averaged metrics provided valuable insight into the relative performance of the different models, but they did not show the differences between the best and worst-performing model chains. The range of the six error metrics is summarized in Table 11 for each PV plant and time horizon.

On average of all plants and horizons, the *nMAE* ranges from 28.3% to 32.6%, which means that the best model chains have 13% less absolute error compared to the worst-performing ones. The average range of *nRMSE* is 46.1% to 52.1%, with a 12% relative difference between the two extremes. The skill scores over persistence (s_p) and climatology-persistence (s_{cp}) are between 33.6–41.2% and 25.9–34.4%, respectively. The best models, on average, have 23% higher s_p and 33% higher s_{cp} skill scores, which is a significant improvement, especially considering that most of the errors are coming from the irradiance forecast [93]. A persistence skill score higher than 40% indicates a good forecast compared to other published results [7]. The range of the error metrics is close to the average range in most plants. However, in Pécs, the difference is almost twice above the average, e.g., the day-ahead *nMAE* and s_{cp} are ranging from 28.0–36.4% and 21.1–35.7%, which means a 23% error reduction and a 69% skill improvement of the best model chain over the worst one, respectively. The design parameters of the Pécs PV plants are similar to the others, but its specific energy production is the lowest among all 16 systems (see Table 8), which results in a high overestimation of the forecasts (average *nMBE* of 8.9%). The higher sensitivity of the forecast accuracy to the model selection in Pécs originates either from this high bias error or from the special local traits of the meteorology or the NWP forecast.

The bias varies in a wide range between −11.3% and 10.6% on average. A previous comparison of nine separation and five transposition models resulted in a bias ranging from –5% to 8% for yearly PV plant simulation [96]. The higher range observed in the present study can be attributed to the higher number of models and modelling steps. The bias of physical modelling is especially important in design simulations of the PV plants, where even several percent difference in the expected energy production can cause a large deviation from the projected financial return. In PV forecasting, bias has only secondary importance, and it can be effectively corrected if some historical data is available. The average variance ratio of the forecasts is between 71.3% and 110.9%; therefore, the under- or overdispersion of the power forecast largely depends on the physical model selection.

Comparing the two time horizons, the intraday forecasts have a 6.9% lower MAE and 6.5% lower RMSE than the day-ahead forecast. The most remarkable improvement is in Kajárpéc 1 with 9.7% MAE and 8.9% RMSE decrease, while the lowest difference is in Paks with 3.7% and 4.0%, respectively. The s_p persistence-based skill score is, on average of all plants, almost identical for both ID and DA horizons, which indicates that the accuracy improvements of the NWP and the reference persistence forecasts are roughly the same. In contrast, the s_{cp} climatology-persistence skill is higher for the ID horizon, which shows that adding the climatology to the persistence reference have higher benefit in the longer time horizon. The s_{cp} difference between the two horizons is higher in 11 of the 16 plants than the s_p difference; therefore, the simple persistence skill score is the more horizon-independent metric for the NWP-based forecasts.

4.3. Model chain performance distribution

The violin plots can best visualize the distribution of the model performance metrics. A sample violin plot displaying the distribution of the day-ahead *nMAE* of all PV plants, grouped by the shading model, is shown in Fig. 3. Each violin plots include a small box plot in the middle, where the white dot indicates the median, the endpoints of the thick grey line are the lower and upper quartile, and the lowest and highest points are the minimum and maximum values, respectively. Moreover, the coloured shapes represent the distribution of the data calculated by a kernel density estimator. The violin plots are produced using the *Seaborn* package for *Python*.

Similar violin plots are created for both time horizons, all six performance metrics, without grouping and grouped by all seven calculation steps. High-resolution versions of all the 96 individual plots are appended as supplementary materials to this paper to provide further details for the readers who are particularly interested in a specific model, metric, or time horizon. These plots contain a large amount of information about the performance of the different models. For example, Fig. 3 shows that including the beam shading improves the overall modelling accuracy, the best model chains calculate with the shading in all locations, and even though the shading calculation itself does not guarantee a good performance, they make the exceptionally high errors less likely by narrowing the range of the results.

The distribution of the *nMAE* results has a positive skew, i.e., the minimum and the lower quartile are closer to the median than the maximum and upper quartile, respectively. The distribution of *nRMSE* is also positively skewed, while both types of skill scores are negatively skewed. This skewness means that the median of these error metrics is closer to the best value than the average; in other words, a randomly chosen model chain will probably have a slightly above-average performance. The bias errors and the variance ratio has a roughly symmetrical distribution. (The violin plots supporting these statements can be found in the supplementary materials.)

4.4. Effect of geographical location

The six PV plants with the lowest forecast error both in terms of *nMAE* and *nRMSE* are Cegléd, Kecel, Kötegyán, Mezőkovácsháza, Paks, and Újkígyós (see Table 11 and Fig. 3). All these six PV plants are located on the Great Hungarian Plain, which is a part of a 100000 km^2 large flatland in the Carpathian Basin. The average nMAE and nRMSE of these six plants are respectively 9.1% and 7.7% lower than the average of the other ten PV plants. The skill scores of these six plants are similar or even smaller than the others; therefore, this good accuracy is mostly due to the less volatile weather and cloud cover in the flatland compared to the hilly terrain.

Among the two locations where irradiance forecast *nRMSE* is known, Nagykőrös can be considered as a representative location of the flatland, while Balatonberény is located in the western, hilly area of the country. The relative difference of 8.4% between the two locations is consistent with the difference in the power forecast errors. Table 12 summarize the average *nRMSE* of the irradiance forecast and the power forecasts of the best and worst model chains for the two groups of PV plants. The RMSE increase due to irradiance-to-power modelling is only 16.0–17.0% if the best model chains are used, but it can range even up to 31.9–32.1% for

Table 11
Minimum, average and maximum values of different metrics for all PV plants and time horizons.

Plant	Hor.	*nMAE, %*			*nMBE, %*			*nRMSE, %*			s_p, %			s_{cp}, %			*F, %*		
		Min	Mean	Max	Min	Mean	Min	Min	Min	Max	Min	Mean	Max	Min	Mean	Max	Min	Mean	Max
Bodajk	DA	30.4	31.7	33.9	−11.1	0.0	10.7	49.4	51.3	55.2	33.0	37.8	40.1	24.6	30.0	32.6	71.4	91.9	110.5
	ID	27.7	28.9	31.3	−13.3	−2.5	8.1	45.8	47.3	50.8	33.8	38.4	40.4	26.8	31.9	34.1	71.0	91.2	109.3
Cegléd	DA	27.7	29.3	32.0	−14.0	−3.2	7.3	45.2	46.8	50.4	34.5	39.2	41.4	26.5	31.7	34.2	69.9	90.2	109.2
	ID	26.4	28.0	30.7	−14.5	−3.8	6.9	43.3	45.0	48.5	34.0	38.7	41.0	26.7	32.0	34.6	70.0	90.1	108.7
Felsőzsolca	DA	30.7	32.0	35.3	−10.3	1.1	11.7	49.8	52.6	57.2	31.2	36.7	40.0	22.5	28.7	32.4	74.4	94.7	113.0
	ID	27.8	29.1	32.5	−10.1	1.3	11.8	46.1	48.6	53.2	28.7	34.9	38.2	21.7	28.5	32.2	75.0	95.5	114.0
Fertőszéplak	DA	31.6	33.0	35.7	−10.7	1.1	12.8	50.5	52.9	57.8	33.8	39.3	42.1	24.9	31.2	34.3	68.9	89.6	108.9
	ID	28.8	30.3	33.0	−12.4	−0.7	10.6	47.2	49.1	53.4	34.7	39.9	42.2	27.2	33.1	35.5	69.2	89.8	108.9
Győrvár 1	DA	32.2	33.5	36.3	−6.7	5.0	16.4	51.4	54.0	58.9	33.2	38.8	41.7	24.0	30.4	33.7	73.0	94.0	113.2
	ID	30.0	31.3	33.9	−8.5	3.1	14.5	48.2	50.3	54.8	34.8	40.2	42.6	26.8	32.9	35.6	72.1	92.6	111.7
Győrvár 2	DA	31.2	32.6	35.0	−8.4	3.1	14.4	50.0	52.2	56.8	34.4	39.7	42.3	25.7	31.7	34.7	71.6	91.9	110.5
	ID	29.2	30.7	33.2	−10.3	1.1	12.3	47.3	49.1	53.5	34.9	40.2	42.4	27.3	33.2	35.7	70.6	90.5	108.9
Kajárpéc 1	DA	31.3	32.7	35.2	−9.9	1.6	13.0	49.8	51.9	56.5	34.3	39.6	42.1	25.4	31.4	34.2	69.5	89.4	108.1
	ID	28.1	29.6	32.1	−12.2	−1.0	10.0	45.7	47.3	51.4	35.8	40.9	43.0	28.4	34.2	36.4	70.4	90.2	108.7
Kajárpéc 2	DA	31.4	32.8	35.1	−11.4	0.1	11.5	50.0	51.9	56.0	35.3	40.1	42.2	26.2	31.7	34.2	68.9	88.8	107.7
	ID	28.3	29.7	32.3	−13.6	−2.4	8.6	46.0	47.5	51.2	36.5	41.1	43.0	29.0	34.2	36.2	70.0	89.8	108.4
Kecel	DA	27.9	29.4	31.9	−12.2	−1.4	9.3	45.4	47.3	51.2	32.9	38.1	40.5	24.9	30.6	33.4	71.1	91.6	110.3
	ID	26.2	27.6	30.3	−13.6	−2.8	8.0	42.7	44.4	48.0	33.0	38.0	40.3	26.1	31.6	34.2	70.8	91.0	109.5
Kötegyán	DA	27.0	28.5	31.3	−15.5	−5.1	5.4	44.6	46.2	48.9	33.0	36.9	39.0	25.8	30.0	32.4	69.7	89.9	109.2
	ID	25.4	26.9	29.7	−14.9	−4.5	6.0	42.5	44.0	47.0	31.0	35.3	37.6	24.7	29.4	31.8	70.4	90.6	109.9
Mezőkovácsháza	DA	26.8	28.4	31.4	−15.4	−5.0	5.4	44.6	46.0	48.7	33.9	37.5	39.5	26.6	30.6	32.8	67.7	87.4	106.1
	ID	25.1	26.7	29.9	−15.5	−5.1	5.4	41.8	43.3	45.8	34.9	38.4	40.5	28.4	32.3	34.6	68.4	88.2	107.2
Nagyvázsony	DA	30.0	31.1	33.5	−8.4	3.0	13.9	47.5	49.7	54.0	36.1	41.1	43.7	27.6	33.3	36.3	71.8	92.4	110.9
	ID	27.3	28.5	30.9	−10.5	0.6	11.3	44.4	46.1	49.9	37.5	42.3	44.4	30.2	35.6	37.9	71.5	91.6	109.9
Paks	DA	26.6	28.0	31.2	−10.7	−0.1	10.9	44.0	46.2	50.4	33.6	39.2	42.1	25.8	32.1	35.3	72.4	94.6	114.3
	ID	25.6	27.0	30.3	−11.8	−1.4	9.5	42.2	44.3	48.6	30.7	36.8	39.8	23.9	30.6	33.9	72.7	94.9	114.5
Pécs	DA	28.0	30.5	36.4	−1.0	9.9	21.3	45.2	49.3	55.4	29.9	37.6	42.8	21.1	29.8	35.7	79.1	102.4	124.7
	ID	26.3	28.6	34.5	−2.9	7.8	18.9	42.7	46.3	52.1	29.8	37.7	42.5	22.3	31.0	36.3	79.4	102.8	125.2
Veszprém	DA	29.9	31.1	33.3	−9.8	1.4	12.0	48.0	50.0	54.1	34.9	39.8	42.2	26.5	32.0	34.7	72.4	93.1	111.9
	ID	27.5	28.6	30.9	−11.8	−0.9	9.8	44.7	46.3	50.0	35.8	40.4	42.5	28.7	33.9	36.1	72.0	92.2	110.4
Újkígyós	DA	27.0	28.6	31.3	−15.0	−4.7	5.7	45.0	46.5	49.5	32.8	36.8	38.9	25.4	29.9	32.2	68.7	88.4	106.9
	ID	25.7	27.2	30.1	−15.2	−4.8	5.6	42.9	44.3	47.1	32.2	36.2	38.3	25.7	30.1	32.3	68.9	88.6	107.4
Average	DA	29.4	30.8	33.7	−10.7	0.4	11.4	47.5	49.7	53.8	33.5	38.6	41.3	25.2	31.0	33.9	71.3	91.9	111.0
	ID	27.2	28.7	31.6	−11.9	−1.0	9.8	44.6	46.5	50.3	33.6	38.7	41.2	26.5	32.1	34.9	71.4	91.8	110.8
Overall average		28.3	29.8	32.6	−11.3	−0.3	10.6	46.1	48.1	52.1	33.6	38.7	41.2	25.9	31.5	34.4	71.3	91.9	110.9

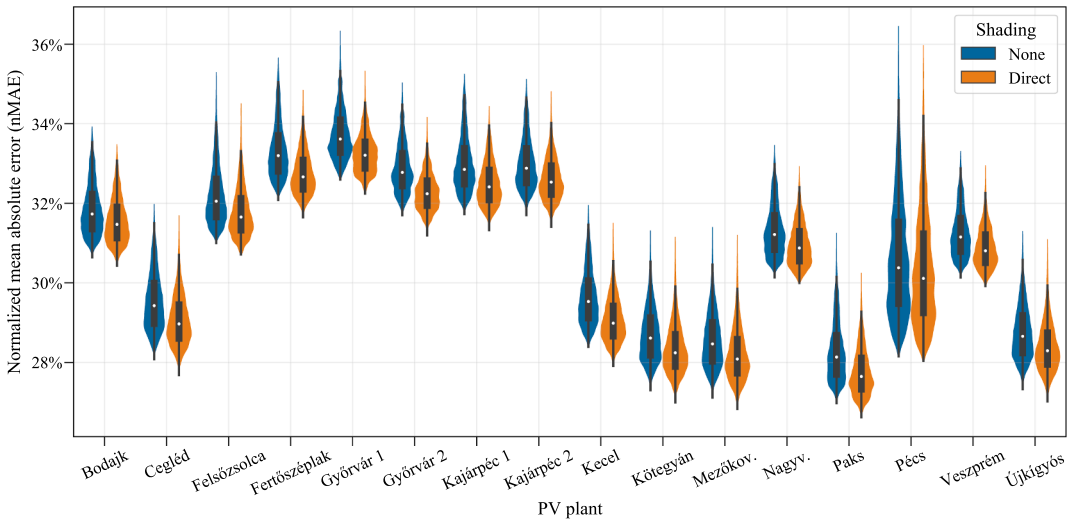

Fig. 3. Violin plots of the normalized mean absolute errors (*nMAE*) grouped by the shading model.

Table 12
Mean-normalized RMSE of the NWP irradiance forecast and the best and worst power forecasts on average for the PV plants in the flatland and the hilly areas.

	Irradiance *nRMSE*	Best power *nRMSE*	Worst power *nRMSE*
Flatland	37.4%	43.8%	49.4%
Hilly areas	41.0%	47.5%	54.1%

the worst-performing model chains. Therefore, almost half of the additional forecast error can be spared by a proper physical model chain selection.

4.5. Best performer model chains

The model chains providing the most accurate forecasts are presented in Table 13 for all locations and time horizons. The accuracy was measured in two terms, the absolute error (*nMAE*) and squared error (*nRMSE*). The overall best performer model chains that have the lowest error on average for all 16 plants are also included in the table.

In terms of absolute error, the C8D1R3T4P1S2I1, C8D7R2T4P1S2I2 model chains are the two most common among the best performers, covering 9 out of the 32 cases. These chains consist of the Starke separation, Mattei temperature, Evans PV, and beam shading model, supplemented by either the Liu-Jordan transposition, physical reflection and constant inverter, or the Perez transposition, Ruiz-Martin reflection and quadratic inverter models. The overall lowest nMAE results from the C8D7R3T2P1S2I1 model chain on both horizons (Starke separation, Muneer transposition, physical reflection, King cell temperature, Evans PV, beam shading, and constant inverter models).

In terms of squared error, the best model chain is one of C6D1R3T1P1S2I1 and C6D1R3T4P1S2I1 in 18 out of the 32 cases. They are made up of the BRL separation, Liu-Jordan transposition, physical reflection, Evans PV, beam shading, and constant inverter model with either the NOCT or the Mattei temperature model. The model chain with the overall lowest *rRMSE* is the C6D1R3T1P1S2I1 (BRL separation, Liu-Jordan transposition, physical reflection, NOCT temperature, Evans PV, beam shading, and constant inverter models).

The best performing model chain mostly depends on the error metric used to measure the accuracy, as there are considerable differences between the lowest MAE and lowest RMSE model chains. The effect of the forecast horizon is small, as the overall best performer model chains are similar for both horizons in terms of both error metrics, and the same is true for the majority of the individual plants.

Table 14 summarize the relative occurrence of each model in the best performing model chains. It includes not only the one best but also the

Table 13
Most accurate model chains for each location and time horizons in terms of absolute (*nMAE*) and squared (*nRMSE*) errors (for the interpretation of the codes, please see Section 3.5).

Plant	Absolute error		Square error	
	Intraday	Day-ahead	Intraday	Day-ahead
Bodajk	C8D7R3T4P1S2I3	C8D7R2T4P1S2I3	C6D10R3T1P1S2I1	C6D1R3T1P1S2I1
Cegléd	C8D7R3T3P1S2I1	C8D7R3T4P1S2I1	C6D1R3T4P1S2I1	C6D1R3T4P1S2I1
Felsőzsolca	C8D7R3T2P1S2I3	C6D3R3T3P4S2I1	C6D1R3T1P1S2I1	C6D1R3T1P1S2I1
Fertőszéplak	C8D7R2T4P1S2I2	C6D9R3T4P4S2I2	C6D1R3T4P1S2I1	C6D1R3T1P1S2I1
Győrvár 1	C8D7R3T4P3S2I1	C8D7R2T3P4S2I1	C6D1R3T1P1S2I3	C6D1R3T1P3S2I1
Győrvár 2	C8D7R3T4P4S2I1	C8D7R2T4P4S2I1	C6D1R3T1P1S2I1	C6D1R3T1P1S2I3
Kajárpéc 1	C8D7R3T3P1S2I2	C8D7R2T4P1S2I3	C6D3R3T1P1S2I1	C6D1R3T1P1S2I1
Kajárpéc 2	C8D7R3T4P1S2I2	C8D7R2T4P1S2I1	C6D10R3T1P1S2I1	C6D1R3T1P1S2I1
Kecel	C8D7R2T3P1S2I1	C8D7R2T3P1S2I1	C6D1R3T4P1S2I1	C6D1R3T1P1S2I1
Kötegyán	C8D1R3T4P1S2I1	C8D1R3T4P1S2I1	C6D8R3T1P1S2I3	C6D8R3T1P1S2I1
Mezőkovácsháza	C8D1R3T4P1S2I1	C8D7R3T3P1S2I1	C6D8R3T1P1S2I1	C6D8R3T1P1S2I1
Nagyvázsony	C8D7R2T4P1S2I2	C6D9R3T5P4S2I2	C6D1R3T1P1S2I1	C6D1R3T1P1S2I1
Paks	C8D1R3T2P1S2I2	C8D1R3T2P1S2I2	C6D1R3T1P1S2I1	C6D1R3T1P1S2I1
Pécs	C6D3R3T1P2S2I1	C6D4R3T1P2S2I1	C6D1R3T1P3S2I1	C6D1R2T1P3S2I1
Veszprém	C8D7R2T4P1S2I2	C8D7R2T4P1S2I2	C6D3R3T1P1S2I3	C6D1R3T1P1S2I1
Újkígyós	C8D1R3T4P1S2I1	C8D1R3T4P1S2I1	C8D1R3T1P1S2I1	C6D1R3T4P1S2I1
Overall	C8D7R3T2P1S2I2	C8D7R3T2P1S2I1	C6D1R3T2P1S2I1	C6D1R3T1P1S2I1

top 1% model chains for all the 32 cases, as finding the absolute best model is often an unrealistic idea, and selecting one of the top performers is mostly enough in the engineering practice.

The most consistent results can be observed by shading modelling, as all of the 32 best and the vast majority of the top 1% model chains include the beam shading calculation. The PHYSICAL reflection, EVANS PV, and CONSTANT inverter models are the most common models among the bests in terms of both error metrics. In the other steps, different models are used for the lowest MAE (STARKE separation, MUNEER transposition, MATTEI temperature) and lowest RMSE (BRL separation, LIU-JORDAN transposition, NOCT temperature). The three inverter models are almost evenly distributed in the top 1%, which indicates that they have a so minor effect on the overall performance that the accuracy of a model chain depends mostly on the other modelling steps.

Comparing the results of Table 10 and Table 14, it is clear that not always the models with the average best scores build up the best model chains. On the one hand, the low average metrics indicate that a given model performs well with all models in the other steps. On the other hand, a high share among the most accurate models shows that a given model can perform outstandingly good with the best models of the other steps.

4.6. Methods for physical model selection

The best-performing model chains for each location can only be selected by hindsight or estimated by historical data. In case no historical data is available for the PV plant of interest (e.g., because it is a new installation), the best model chain can be estimated from the historical data of nearby power plants. The effectiveness of this model selection method can be examined through the difference of the individual and overall most accurate model chains for each plant. Finally, if neither local nor regional historical data are available, one can use the simplest possible model chain or perform a thorough literature review to find the models that performed the best in different benchmark studies.

Table 14
Share of the different models among the best and the top 1% model chains in terms of absolute (*nMAE*) and squared (*nRMSE*) errors for all plants and horizons.

		Absolute error		Square error	
		Best	Top 1%	Best	Top 1%
Separation	ERBS	0%	1%	0%	12%
	SKARTVEIT-OLSETH	0%	1%	0%	3%
	DISC	0%	3%	0%	0%
	DIRINT	0%	2%	0%	0%
	DIRINDEX	0%	0%	0%	0%
	BRL	16%	41%	97%	70%
	ENGERER	0%	4%	0%	3%
	STARKE	84%	47%	3%	3%
	ABREU	0%	1%	0%	9%
Transposition	LIU-JORDAN	22%	11%	75%	63%
	STEVEN	0%	0%	0%	0%
	HAY	6%	10%	6%	9%
	WILLMOT	3%	5%	0%	1%
	SKARTVEIT-OLSETH	0%	8%	0%	3%
	GUEYMARD	0%	6%	0%	0%
	MUNEER	63%	22%	0%	2%
	KLUCHER	0%	15%	13%	10%
	PEREZ	6%	14%	0%	2%
	REINDL	0%	11%	6%	9%
Refl.	None	0%	1%	0%	17%
	MARTIN-RUIZ	34%	38%	3%	20%
	PHYSICAL	66%	61%	97%	63%
Temperature	NOCT	6%	9%	84%	41%
	KING	9%	9%	0%	26%
	FAIMAN	22%	20%	0%	13%
	MATTEI	59%	33%	16%	12%
	SKOPLAKI	3%	30%	0%	8%
PV module	EVANS	72%	53%	91%	62%
	HULD	6%	7%	0%	1%
	SINGLE DIODE 4	3%	12%	9%	18%
	SINGLE DIODE 5	19%	28%	0%	19%
Shd.	None	0%	3%	0%	27%
	BEAM SHADING	100%	97%	100%	73%
Inverter	CONSTANT	56%	36%	88%	36%
	QUADRATIC	31%	36%	0%	32%
	DRIESSE	13%	28%	13%	32%

The average performance metrics of the forecasts performed by the models selected with these four approaches are summarized in Table 15. The first two rows are the average of the forecasts created for each plant and horizon with the model chains that are most accurate for the given case (see Table 13). The next two rows show the performance of the model chains with the overall lowest errors (C8D10R3T2P1S2I2 for absolute and C6D1R3T1P1S2I1 for squared error). The simplest model chain is the C1D1R1T1P1S1I1, which includes the EBRS separation, LIU-JORDAN transposition, NOCT cell temperature, EVANS PV, and CONSTANT inverter efficiency model without reflection and shading calculation. Most of these models are just one equation; thus, the full model chain can be programmed in less than 10 lines of code. The best model chain that can be constructed based on the literature is C8D9R3T4P4S2I3, which consists of the STARKE separation model (it outperforms the ENGERER model in [31], which is best of 140 models in [30]), the PEREZ transposition model (best of 26 models in [46]), the MATTEI cell temperature model (best of 8 models in [68]), the most detailed reflection (PHYSICAL), PV (SINGLE DIODE 5) and inverter (DRIESSE) models, and includes the shading losses.

The error of overall best model chains is only slightly (0.7% for MAE and 0.2% for RMSE) higher than the individual bests. Therefore, relying on the data of other power plants in the same region is a sound basis for the physical model selection. The simple model performs well in terms of RMSE, with only 1.2% higher error compared to the best models; however, it has 8.1% higher MAE compared to the best values. In contrast, the literature best model has only 2.8% higher MAE, but 6.2% higher RMSE compared to the respective individual best. In case the MAE is a better representation of the value of the forecast, the forecaster should use a model chain consisting of the best models that can be found in the literature. However, if the RMSE is considered as the more relevant error metric, a simple PV model may perform better than a detailed one.

The first four rows of Table 15 can be classified into two groups, the low-MAE and the low-RMSE model chains. The bias and variance are also significantly different in the two groups. The low-MAE model chains have low *nMBE* (1.0–2.5%) but a higher variance ratio (95.8–97.7%). The absolute error is equally sensitive to lower and higher errors; thus, even a moderate bias can considerably increase the MAE. In contrast, the low-RMSE model chains have a higher bias (−3.6% to –5.4%) and lower variance ratio (78.7–83.0%). The RMSE is more sensitive to the higher errors; therefore, it benefits from the less extreme power values of an under-dispersed forecast.

4.7. Effect of the wind speed forecast

The irradiance is the primary input of the PV forecasts, while the ambient temperature forecasts are also widely accessible as they can be obtained even from public sources with acceptable accuracy. However, even though the wind speed forecast is available among the NWP outputs, the weather services often charge extra cost for it due to its immense value in the wind power forecasts. In physical PV forecasting, the wind speed is only used in the cell temperature calculation; a higher wind speed results in a lower temperature and a slightly higher power output. In case no wind forecast is available, the models can still be used with constant wind speed. This constant speed can be the long-term average wind speed the area of interest, which is around 3 m/s for Hungary (ranging between 2 m/s and 4 m/s according to the Hungarian

Table 15
Average error and performance metrics of 6 different model chains.

	Hor.	*nMAE*	*nMBE*	*nRMSE*	s_p	s_{cp}	*F*
Individual best *nMAE* (see Table 13)	DA	29.4%	2.2%	49.1%	39.4%	31.8%	97.4%
	ID	27.2%	1.3%	45.9%	39.5%	33.0%	97.7%
Individual best *nRMSE* (see Table 13)	DA	30.7%	−3.7%	47.5%	41.3%	33.9%	79.9%
	ID	28.3%	−3.6%	44.6%	41.2%	34.9%	83.0%
Overall best *nMAE* (C8D10R3T2P1S2I2)	DA	29.6%	2.5%	49.0%	39.4%	31.8%	95.9%
	ID	27.4%	1.0%	45.7%	39.7%	33.2%	95.8%
Overall best *nRMSE* (C6D1R3T1P1S2I1)	DA	30.9%	−4.1%	47.6%	41.2%	33.8%	78.7%
	ID	29.0%	−5.4%	44.7%	41.0%	34.7%	78.7%
Simple (C1D1R1T1P1S1I1)	DA	31.6%	−2.3%	48.1%	40.6%	33.2%	78.5%
	ID	29.5%	−3.7%	45.2%	40.4%	34.0%	78.6%
Literature best (C8D9R3T4P4S2I3)	DA	30.2%	5.6%	50.6%	37.5%	29.6%	102.6%
	ID	28.0%	4.1%	47.2%	37.8%	31.1%	102.5%

Meteorological Service). Alternatively, if no local wind data is available, the forecasts can also be calculated with a 1 m/s wind speed corresponding to the NOCT conditions of the modules.

The verification of all model chains for all locations and horizons was also performed without the wind speed forecast data using constant 1 m/s and 3 m/s values. The average performance metrics for all model chains, plants, and horizons are listed in Table 16. The constant wind speed increases the average absolute error and bias but decreases the squared error and variance ratio. The difference is practically negligible if the long-term average 3 m/s is used, and it is still minor for the constant 1 m/s. The constant 1 m/s wind speed changed the average bias from −0.3% to −1.3%, as the actual wind speed is typically higher than 1 m/s, and the small value on average underestimates the cooling effect to the wind and thus also the power output. The average variance ratio decreases from 91.9% to 89.1% for the 1 m/s wind speed case, which meets the expectations that the wind forecast contributes to the variability of the forecast. The tendencies are similar if only the best model chains are considered; the MAE increases by 0.038% and 0.011%, while the RMSE decreases by 0.021% and 0.011% on the average of all plants and horizons in the case of the 1 m/s and 3 m/s wind speeds, respectively.

The wind speed forecast increases the dispersion and improves the MAE of the forecast, but the difference is so small that it mostly does not worth the extra money or effort to include it in the power forecast. If RMSE is the error metric of interest, it is even beneficial to use a constant low wind speed instead of wind forecasts. These results correspond to the observation that wind speed has only a weak correlation to the power output [27]. However, as the wind speed is typically low in Hungary, its effect may be slightly higher in more windy regions.

4.8. Further discussion

The BRL model is proven to be one of the best separation models in all main criteria and locations. The cloud enhancement effect, i.e., the temporary increase of the global irradiance over the clear sky irradiance level, resulting in an increased diffuse fraction for high clearness index [97], is not considered in this model. Cloud enhancement only appears in high-resolution measurement data, and it is not present in the 15-min resolution NWP forecasts, which can be a possible reason for the good performance of BRL on NWP data, even though it was overperformed by several other models in a worldwide validation study based on 1-min measurement data [30]. The DIRINDEX model has the highest errors in the present study, but the performance of this model largely depends on the clear sky model. In this study, DIRINDEX is paired with the Ineichen-Perez clear sky model [39], as implemented in the *pvlib* Python package [29]. The DIRINDEX model may perform better if used with another clear sky model; however, the more complex models require a larger number of atmospheric parameters that are not always available in the irradiance forecasts [98].

The performance of the Single diode PV models depends on not only the number of parameters but also the parameter estimation method. Improved accuracy is expected if the parameters can be estimated from experimental data instead of the datasheet values [25]. The measurement-estimated parameters of a large number of modules can be found in the resources of the System Advisor Model (SAM) software, which can be accessed from a public *GitHub* repository (https://github.com/NREL/SAM/tree/develop/deploy/libraries). However, there is no guarantee that the modules of interest are included in this database, and performing experiments by the plant owners are not justified by the slight accuracy improvement, especially as the PV model is not the most critical step of the calculation process. The inverter models have the lowest effect on the overall forecast accuracy, but the voltage-dependent Driesse model performed even slightly worse than the simpler ones. Even though the voltage dependence is essential to properly reproduce the efficiency curves supplied in the inverter datasheets, the better performance of the voltage-independent models for measured data has already shown in [99].

The *pvlib* Python package and the *PV_LIB* Matlab Toolbox, both developed in the frame of the PV Performance Modelling Collaborative (PVPMC) facilitated by the Sandia National Laboratory, are useful tools for physical modelling of PV systems [100]. The *pvlib* includes fewer models and has a slightly different model chain concept compared to this study as PVPMC mainly focuses on the design simulation of PV plants, but it can still be used for physical power forecasting with only a small programming effort. In this study, *pvlib* was only used for the calculation of the position of the Sun and the DIRINT and DIRINDEX separation models (including the Ineichen-Perez clear sky model). The other models were coded in Python by the authors due to the need for better calculation effectiveness. (The total runtime of the 1,036,800 verifications in the first working version was more than one week using an average PC, which was reduced to 12 h by code refactoring using lower-level data formats.)

The presented results do not express the overall accuracy of the models, but only characterize their performance in power forecasting applications. This paper does not call into question the findings of the previous verification and benchmark studies performed on research-

Table 16
Average error and performance metrics with forecasted and constant 1 m/s and 3 m/s wind speeds.

	nMAE	*nMBE*	*nRMSE*	s_p	s_{cp}	*F*
Wind forecast	29.753%	−0.292%	48.061%	38.679%	31.550%	91.863%
1 m/s constant wind speed	29.871%	−1.347%	47.804%	39.001%	31.910%	89.131%
3 m/s constant wind speed	29.757%	−0.304%	48.026%	38.723%	31.599%	91.791%

grade measurement data. Instead, the results highlight that not always the ideally most accurate models are the bests in practical applications, especially for power forecasting based on inherently erroneous weather predictions. Gueymard has already shown in 2009 that not always the most accurate transposition models have the best results when they are used on imperfect data [23].

The lack of operational aspects is a common problem in many forecasting papers [101]. The power forecasts presented in this paper are fully operational, especially from the perspective PV plant owners: NWP data is purchased once a day from a local meteorological service, which is used for providing the 15-min day-ahead forecast before the regular deadline of 10 or 12 a.m., and also the one-time intraday update without any additional data requirements and costs. In practice, further intraday forecast refinements are possible up to several hours ahead (2.5 h in Hungary), which can be based on irradiance forecasts derived from sky and satellite imagery that are typically more accurate than NWP for less than 3–4 h forecast horizons [102]. These short-term power forecasts are out of the scope of this paper; however, the presented physical model chains can also be used in this time horizon for the irradiance-to-power conversion.

The MAE and RMSE are two conflicting error metrics, as no model can be found to perform among the bests in both terms. The lowest MAE is provided by the models that are more detailed and typically performed well in previous comparative studies. In contrast, the lowest RMSE is resulted by simple models, and it is coupled with a heavily under-dispersed forecast. Even though RMSE is widely considered as the most important metric of the forecast accuracy [3], it is not clear whether an under-dispersed forecast with almost no extremes can indeed provide the highest market value. Application of a smoothing post-processing technique (e.g., moving average) reduces the variance of the forecast. Therefore, further research is required to discover whether or not a smoothed output of a sophisticated physical model chain can outperform the simple model chains that yielded the lowest RMSE in the present study. The imbalance penalties paid by the PV plant owners are mostly proportional to the absolute error; hence, MAE is the better indicator from their point of view [90].

The presented power forecasts are deterministic, i.e., they assign a single value for each timestep over the forecast horizon. In contrast, probabilistic forecasts also provide a prediction interval or a predictive density to describe the uncertainties of the forecast [101]. Probabilistic power forecasts can be created from probabilistic irradiance forecasts with the model chains presented in this study, but they only cover the uncertainties coming from the irradiance forecasting. The additional uncertainties of the irradiance to power calculation can be accounted for by probabilistic model chains, as probabilistic separation [103] and transposition [104] models are already available in the literature. Alternatively, probabilistic model chains can also be constructed by ensemble modelling, e.g., using ensemble model output statistics (EMOS) for multiple model chains, similarly as implemented for transposition models in [104]. Probabilistic solar power forecasting is a promising field for further research.

The main limitation of the present study is that the models are only verified for only the temperate climatic region and one NWP forecast provider. A worldwide verification could show how the local climate and weather characteristics influence the difference between the model chains and the optimal model selection. Moreover, testing the models for different NWP or even CMV-based irradiance forecasts will reveal whether similar or different model chains should be used for the same plants for the different irradiance forecasts. The main obstacle of such studies is the lack of reliable production data of operational PV plants with known design parameters, which is also the main reason for the underrepresentation of the power forecast papers in the solar forecasting literature [95]. Further research areas include the analysis of the effect of post-processing and hybridization techniques on the importance and methods of the physical model selection and improvement potential of forecast accuracy.

5. Conclusion

This study presents the most extensive comparison of the models for physical photovoltaic (PV) power forecasting calculation from numerical weather prediction data by now. The 32,400 model chains – composed of all combinations of the carefully selected submodels (nine separation, ten transposition, three reflection, five cell temperature, four PV performance, two shading, and three inverter models) – are verified for 16 PV plants for intraday and day-ahead time horizons. The six main performance metrics, following the latest recommendations for forecast verifications, are the mean absolute error (MAE), mean bias error (MBE), root mean square error (RMSE), persistence and climatology-persistence skill scores, and the variance ratio. The detailed evaluation of the 1,036,800 individual verification results, each calculated for one-year 15-min resolution datasets of around 17,000 valid entries, led to the following conclusions:

- The models acknowledged as the best in the literature do not provide the most accurate results in power forecast calculations.
- The two most critical calculation steps, i.e., where the selection of the best model has the highest effect on the accuracy, are the beam and diffuse separation and tilted irradiance transposition models. The selection of the inverter model has the lowest effect on forecast accuracy.
- The difference between the most and least accurate model chains is 13% in MAE, 12% in RMSE, and 23–33% in the two skill scores for a PV plant on average. Considering that most of the forecast errors are coming from the irradiance prediction [93], and even one percent accuracy change has a considerable market value [12], the selection of the best model chain has high importance.
- On average, the *nRMSE* of power forecast created by the best and worst model chains are respectively 16.8% and 32.6% higher compared to the *nRMSE* of the irradiance forecast, which means that a good model selection can spare almost half of the additional error.
- The model chains with lowest MAE consist of the Starke separation model, Muneer transposition model, Martin-Ruiz or physical reflection model, Faiman or Mattei cell temperature model, Evans PV performance model, beam shading calculation, and constant or quadratic inverter efficiency models. The model chains with the lowest RMSE induce the BLR separation model, Liu-Jordan transposition model, physical reflection calculation, NOCT cell temperature model, Evans PV model, beam shading calculation, and constant inverter efficiency.
- Mean absolute error and mean square error are conflicting metrics, thus further study is required to identify which represents the value of the forecast better. The more elaborated models are required for the lowest MAE, while the simplest ones are enough for the lowest RMSE, though the latter leads to largely under-dispersed forecasts.
- Wind speed forecasts slightly improve the MAE but increase the RMSE of the power forecast compared to the calculation with a constant long-term average wind speed. The overall benefits of the wind forecast data are marginal.
- The six PV plants located in the flatlands of the Great Hungarian Plain have 8–9% lower power forecast errors compared to the other ten plants built on areas with more diverse topography.

Further research is suggested regarding the post-processing and hybridization of the physical power forecast models. Extending the presented verification for more climate zones and irradiance forecast providers would be useful to deepen the understanding of the physical modelling approach. The main obstacle of such studies is the lack of accessible PV power production and irradiance forecast data; thus, the authors are open to collaborations in such research areas.

CRediT authorship contribution statement

Martin János Mayer: Conceptualization, Methodology, Software, Validation, Formal analysis, Data curation, Visualization, Writing - original draft. **Gyula Gróf:** Supervision.

Declaration of Competing Interest

The authors declare that they have no known competing financial interests or personal relationships that could have appeared to influence the work reported in this paper.

Acknowledgement

The authors express their gratitude to Mihály Szűcs, Gabriella Szépszó and the employees of the Hungarian Meteorological Service for providing the AROME numerical weather prediction data, and Norbert Péter and Róbert Csapó from the MVM Green Generation Ltd. for the PV plant design and production data. This research was financed in part by project no. FIEK_16-1-2016-0007 that has been implemented with the support provided from the National Research, Development and Innovation Fund of Hungary, financed under the FIEK_16 funding scheme, and it has been supported by the NRDI Fund (TKP2020 NC, Grant No. BME-NCS) based on the charter of bolster issued by the NRDI Office under the auspices of the Ministry for Innovation and Technology.

Appendix A. Supplementary data

Supplementary data to this article can be found online at https://doi.org/10.1016/j.apenergy.2020.116239.

References

[1] Renewable Energy Policy Network for the 21st Century. Renewables 2018 Global Status Report. Paris; 2018. doi:978-3-9818911-3-3.
[2] Zepter JM, Weibezahn J. Unit commitment under imperfect foresight – The impact of stochastic photovoltaic generation. Appl Energy 2019;243:336–49. https://doi.org/10.1016/j.apenergy.2019.03.191.
[3] Blaga R, Sabadus A, Stefu N, Dughir C, Paulescu M, Badescu V. A current perspective on the accuracy of incoming solar energy forecasting. Prog Energy Combust Sci 2019;70:119–44. https://doi.org/10.1016/j.pecs.2018.10.003.
[4] Yang D, Kleissl J, Gueymard CA, Pedro HTC, Coimbra CFM. History and trends in solar irradiance and PV power forecasting: A preliminary assessment and review using text mining. Sol Energy 2018;168:60–101. https://doi.org/10.1016/j.solener.2017.11.023.
[5] Ulbricht R, Fischer U, Lehner W, Donker H. First steps towards a systematical optimized strategy for solar energy supply forecasting. In: Eur. Conf. Mach. Learn. Princ. Pract. Knowl. Discov. Databases, ECMLPKDD 2013; 2013. p. 2013.
[6] Lorenz E, Heinemann D. Prediction of Solar Irradiance and Photovoltaic Power. Compr. Renew. Energy, vol. 1, Elsevier; 2012. p. 239–92. doi: 10.1016/B978-0-08-087872-0.00114-1.
[7] Antonanzas J, Osorio N, Escobar R, Urraca R, Martinez-de-Pison FJ, Antonanzas-Torres F. Review of photovoltaic power forecasting. Sol Energy 2016;136:78–111. https://doi.org/10.1016/j.solener.2016.06.069.
[8] Li Y, He Y, Su Y, Shu L. Forecasting the daily power output of a grid-connected photovoltaic system based on multivariate adaptive regression splines. Appl Energy 2016;180:392–401. https://doi.org/10.1016/j.apenergy.2016.07.052.
[9] Leva S, Dolara A, Grimaccia F, Mussetta M, Ogliari E. Analysis and validation of 24 hours ahead neural network forecasting of photovoltaic output power. Math Comput Simul 2017;131:88–100. https://doi.org/10.1016/j.matcom.2015.05.010.
[10] Wang K, Qi X, Liu H. A comparison of day-ahead photovoltaic power forecasting models based on deep learning neural network. Appl Energy 2019;251. https://doi.org/10.1016/j.apenergy.2019.113315.
[11] Theocharides S, Makrides G, Livera A, Theristis M, Kaimakis P, Georghiou GE. Day-ahead photovoltaic power production forecasting methodology based on machine learning and statistical post-processing. Appl Energy 2020;268:115023. https://doi.org/10.1016/j.apenergy.2020.115023.
[12] Antonanzas J, Pozo-Vázquez D, Fernandez-Jimenez LA, Martinez-de-Pison FJ. The value of day-ahead forecasting for photovoltaics in the Spanish electricity market. Sol Energy 2017;158:140–6. https://doi.org/10.1016/j.solener.2017.09.043.
[13] Sobri S, Koohi-Kamali S, Rahim NA. Solar photovoltaic generation forecasting methods: A review. Energy Convers Manag 2018;156:459–97. https://doi.org/10.1016/j.enconman.2017.11.019.
[14] Almeida MP, Muñoz M, de la Parra I, Perpiñán O. Comparative study of PV power forecast using parametric and nonparametric PV models. Sol Energy 2017;155:854–66. https://doi.org/10.1016/j.solener.2017.07.032.
[15] Wolff B, Kühnert J, Lorenz E, Kramer O, Heinemann D. Comparing support vector regression for PV power forecasting to a physical modeling approach using measurement, numerical weather prediction, and cloud motion data. Sol Energy 2016;135:197–208. https://doi.org/10.1016/j.solener.2016.05.051.
[16] Schmelas M, Feldmann T, da Costa Fernandes J, Bollin E. Photovoltaics energy prediction under complex conditions for a predictive energy management system. J Sol Energy Eng 2015;137:1–10. https://doi.org/10.1115/1.4029378.
[17] Ogliari E, Dolara A, Manzolini G, Leva S. Physical and hybrid methods comparison for the day ahead PV output power forecast. Renew Energy 2017;113:11–21. https://doi.org/10.1016/j.renene.2017.05.063.
[18] Yang D, Wu E, Kleissl J. Operational solar forecasting for the real-time market. Int J Forecast 2019;35:1499–519. https://doi.org/10.1016/j.ijforecast.2019.03.009.
[19] Lorenz E, Scheidsteger T, Hurka J. Regional PV power prediction for improved grid integration. Prog Photovoltaics Res Appl 2011;19:757–71. https://doi.org/10.1002/pip.1033.
[20] Saint-Drenan YM, Bofinger S, Fritz R, Vogt S, Good GH, Dobschinski J. An empirical approach to parameterizing photovoltaic plants for power forecasting and simulation. Sol Energy 2015;120:479–93. https://doi.org/10.1016/j.solener.2015.07.024.
[21] Holland N, Pang X, Herzberg W, Karalus S, Bor J, Lorenz E. Solar and PV forecasting for large PV power plants using numerical weather models, satellite data and ground measurements. In: 2019 IEEE 46th Photovolt. Spec. Conf. IEEE; 2019. p. 1609–14. https://doi.org/10.1109/PVSC40753.2019.8980496.
[22] Amaro e Silva R, Brito MC. Spatio-temporal PV forecasting sensitivity to modules' tilt and orientation. Appl Energy 2019;255:113807. https://doi.org/10.1016/j.apenergy.2019.113807.
[23] Gueymard CA. Direct and indirect uncertainties in the prediction of tilted irradiance for solar engineering applications. Sol Energy 2009;83:432–44. https://doi.org/10.1016/j.solener.2008.11.004.
[24] Pelland S, Galanis G, Kallos G. Solar and photovoltaic forecasting through post-processing of the Global Environmental Multiscale numerical weather prediction model. Prog Photovoltaics Res Appl 2013;21:284–96. https://doi.org/10.1002/pip.1180.
[25] Dolara A, Leva S, Manzolini G. Comparison of different physical models for PV power output prediction. Sol Energy 2015;119:83–99. https://doi.org/10.1016/j.solener.2015.06.017.
[26] Mayer MJ, Szilágyi A, Gróf G. Environmental and economic multi-objective optimization of a household level hybrid renewable energy system by genetic algorithm. Appl Energy 2020;269:115058. https://doi.org/10.1016/j.apenergy.2020.115058.
[27] Ahmed R, Sreeram V, Mishra Y, Arif MD. A review and evaluation of the state-of-the-art in PV solar power forecasting: Techniques and optimization. Renew Sustain Energy Rev 2020;124:109792. https://doi.org/10.1016/j.rser.2020.109792.
[28] Reda I, Andreas A. Solar position algorithm for solar radiation applications. Sol Energy 2004;76:577–89. https://doi.org/10.1016/j.solener.2003.12.003.
[29] Holmgren WF, Hansen CW, Mikofski MA. Pvlib Python: a Python package for modeling solar energy systems. J Open Source Softw 2018;3:884. https://doi.org/10.21105/joss.00884.
[30] Gueymard CA, Ruiz-Arias JA. Extensive worldwide validation and climate sensitivity analysis of direct irradiance predictions from 1-min global irradiance. Sol Energy 2016;128:1–30. https://doi.org/10.1016/j.solener.2015.10.010.
[31] Yang D, Boland J. Satellite-augmented diffuse solar radiation separation models. J Renew Sustain Energy 2019;11:023705. https://doi.org/10.1063/1.5087463.
[32] Yang D, Alessandrini S, Antonanzas J, Antonanzas-Torres F, Badescu V, Beyer HG, et al. Verification of deterministic solar forecasts. Sol Energy 2020:1–18. https://doi.org/10.1016/j.solener.2020.04.019.
[33] Erbs DG, Klein SA, Duffie JA. Estimation of the diffuse radiation fraction for hourly, daily and monthly-average global radiation. Sol Energy 1982;28:293–302. https://doi.org/10.1016/0038-092X(82)90302-4.
[34] Skartveit A, Olseth JA. A model for the diffuse fraction of hourly global radiation. Sol Energy 1987;38:271–4. https://doi.org/10.1016/0038-092X(87)90049-1.
[35] Bird RE, Hulstrom RL. A simplified clear sky model for direct and diffuse insolation on horizontal surfaces. Golden, CO; 1981.
[36] Kasten F, Young AT. Revised optical air mass tables and approximation formula. Appl Opt 1989;28:4735–8.
[37] Perez RR, Ineichen P, Maxwell EL, Seals RD, Zelenka A. Dynamic global-to-direct irradiance conversion models. ASHRAE Trans 1992;98:354–69.
[38] Perez R, Ineichen P, Moore K, Kmiecik M, Chain C, George R, et al. A new operational model for satellite-derived irradiances: Description and validation. Sol Energy 2002;73:307–17. https://doi.org/10.1016/S0038-092X(02)00122-6.
[39] Ineichen P, Perez R. A new airmass independent formulation for the linke turbidity coefficient. Sol Energy 2002;73:151–7. https://doi.org/10.1016/S0038-092X(02)00045-2.
[40] Ridley B, Boland J, Lauret P. Modelling of diffuse solar fraction with multiple predictors. Renew Energy 2010;35:478–83. https://doi.org/10.1016/j.renene.2009.07.018.
[41] Engerer NA. Minute resolution estimates of the diffuse fraction of global irradiance for southeastern Australia. Sol Energy 2015;116:215–37. https://doi.org/10.1016/j.solener.2015.04.012.
[42] Threlkeld J, Jordan R. Direct solar radiation available on clear days. Heat Piping Air Cond 1957;29(12):135–45.

[43] Bright JM, Engerer NA. Engerer2: Global re-parameterisation, update, and validation of an irradiance separation model at different temporal resolutions. J Renew Sustain Energy 2019;11:18. https://doi.org/10.1063/1.5097014.

[44] Starke AR, Lemos LFL, Boland J, Cardemil JM, Colle S. Resolution of the cloud enhancement problem for one-minute diffuse radiation prediction. Renew Energy 2018;125:472–84. https://doi.org/10.1016/j.renene.2018.02.107.

[45] Abreu EFM, Canhoto P, Costa MJ. Prediction of diffuse horizontal irradiance using a new climate zone model. Renew Sustain Energy Rev 2019;110:28–42. https://doi.org/10.1016/j.rser.2019.04.055.

[46] Yang D. Solar radiation on inclined surfaces: Corrections and benchmarks. Sol Energy 2016;136:288–302. https://doi.org/10.1016/j.solener.2016.06.062.

[47] Liu B, Jordan R. Daily insolation on surfaces tilted towards equator. ASHRAE J 1961;3:53–9.

[48] Steven MD, Unsworth MH. The diffuse solar irradiance of slopes under cloudless skies. Q J R Meteorol Soc 1979;105:593–602.

[49] Hay JE, Davies JA. Calculation of the solar irradiance incident on an inclined surface. In: Hay JE, Won TK, editors. First Can. Sol. Radiat. Data Work., Toronto, Ontario, Canada; 1980. p. 59–72.

[50] Willmott CJ. On the climatic optimization of the tilt and azimuth of flat-plate solar collectors. Sol Energy 1982;28:205–16. https://doi.org/10.1016/0038-092X(82)90159-1.

[51] Skartveit A, Asle Olseth J. Modelling slope irradiance at high latitudes. Sol Energy 1986;36:333–44. https://doi.org/10.1016/0038-092X(86)90151-9.

[52] Gueymard C. An anisotropic solar irradiance model for tilted surfaces and its comparison with selected engineering algorithms. Sol Energy 1987;38:367–86. https://doi.org/10.1016/0038-092X(87)90009-0.

[53] Gueymard CA. Erratum to "An anisotropic solar irradiance model for tilted surfaces and its comparison with selected engineering algorithms". Sol Energy 1988;40:175. https://doi.org/10.1016/0038-092X(88)90087-4.

[54] Muneer T. Solar radiation model for Europe. Build Serv Eng Res Technol 1990;11:153–63. https://doi.org/10.1177/014362449001100405.

[55] Gracia AM, Huld T. Performance comparison of different models for the estimation of global irradiance on inclined surfaces: Validation of the model implemented in PVGIS; 2013. doi: 10.2790/91554.

[56] Klucher TM. Evaluation of models to predict insolation on tilted surfaces. Sol Energy 1979;23:111–4. https://doi.org/10.1016/0038-092X(79)90110-5.

[57] Perez R, Stewart R, Seals R, Guertin T. The development and verification of the perez diffuse radiation model. Sandia Rep 1988.

[58] Perez R, Ineichen P, Seals R, Michalsky J, Stewart R. Modeling daylight availability and irradiance components from direct and global irradiance. Sol Energy 1990;44:271–89. https://doi.org/10.1016/0038-092X(90)90055-H.

[59] Reindl DT, Beckman WA, Duffie JA. Evaluation of hourly tilted surface radiation models. Sol Energy 1990;45:9–17. https://doi.org/10.1016/0038-092X(90)90061-G.

[60] Duffie JA, Beckman WA. Solar engineering of thermal processes, 2nd ed. Hoboken, NJ, USA: John Wiley & Sons, Inc.; 2013. doi:10.1002/9781118671603.

[61] Souka AF, Safwat HH. Determination of the optimum orientations for the double-exposure, flat-plate collector and its reflectors. Sol Energy 1966;10:170–4. https://doi.org/10.1016/0038-092X(66)90004-1.

[62] Martin N, Ruiz JM. Calculation of the PV modules angular losses under field conditions by means of an analytical model. Sol Energy Mater Sol Cells 2001;70:25–38. https://doi.org/10.1016/S0927-0248(00)00408-6.

[63] King DL, Boyson WE, Kratochvil JA. Photovoltaic array performance model. Sandia Rep No 2004-3535 2004;8:1–19. doi:10.2172/919131.

[64] Marion B. Numerical method for angle-of-incidence correction factors for diffuse radiation incident photovoltaic modules. Sol Energy 2017;147:344–8. https://doi.org/10.1016/j.solener.2017.03.027.

[65] Santiago I, Trillo-Montero D, Moreno-Garcia IM, Pallarés-López V, Luna-Rodríguez JJ. Modeling of photovoltaic cell temperature losses: A review and a practice case in South Spain. Renew Sustain Energy Rev 2018;90:70–89. https://doi.org/10.1016/j.rser.2018.03.054.

[66] Mattei M, Notton G, Cristofari C, Muselli M, Poggi P. Calculation of the polycrystalline PV module temperature using a simple method of energy balance. Renew Energy 2006;31:553–67. https://doi.org/10.1016/j.renene.2005.03.010.

[67] Kikumoto H, Ooka R, Sugawara H, Lim J. Observational study of power-law approximation of wind profiles within an urban boundary layer for various wind conditions. J Wind Eng Ind Aerodyn 2017;164:13–21. https://doi.org/10.1016/j.jweia.2017.02.003.

[68] Schwingshackl C, Petitta M, Wagner JE, Belluardo G, Moser D. Wind effect on PV module temperature: Analysis of different techniques for an accurate estimation. Energy Procedia 2013;40:77–86. https://doi.org/10.1016/j.egypro.2013.08.010.

[69] Ross AG. Flat-plate photovoltaic module and array engineering. In: Proc. 1982 Annu. Meet. Am. Sect. Int. Sol. Energy Soc., Houston, Texas; 1982. p. 4321–4.

[70] Faiman D. Assessing the outdoor operating temperature of photovoltaic modules. Prog Photovoltaics Res Appl 2008;16:307–15. https://doi.org/10.1002/pip.813.

[71] Koehl M, Heck M, Wiesmeier S, Wirth J. Modeling of the nominal operating cell temperature based on outdoor weathering. Sol Energy Mater Sol Cells 2011;95:1638–46. https://doi.org/10.1016/j.solmat.2011.01.020.

[72] Skoplaki E, Boudouvis AG, Palyvos JA. A simple correlation for the operating temperature of photovoltaic modules of arbitrary mounting. Sol Energy Mater Sol Cells 2008;92:1393–402. https://doi.org/10.1016/j.solmat.2008.05.016.

[73] Amillo AMG, Huld T, Vourlioti P, Müller R, Norton M. Application of satellite-based spectrally-resolved solar radiation data to PV performance studies. Energies 2015;8:3455–88. https://doi.org/10.3390/en8053455.

[74] Lindsay N, Libois Q, Badosa J, Migan-Dubois A, Bourdin V. Errors in PV power modelling due to the lack of spectral and angular details of solar irradiance inputs. Sol Energy 2020;197:266–78. https://doi.org/10.1016/j.solener.2019.12.042.

[75] Huld T, Friesen G, Skoczek A, Kenny RP, Sample T, Field M, et al. A power-rating model for crystalline silicon PV modules. Sol Energy Mater Sol Cells 2011;95:3359–69. https://doi.org/10.1016/j.solmat.2011.07.026.

[76] de la Parra I, Muñoz M, Lorenzo E, García M, Marcos J, Martínez-Moreno F. PV performance modelling: A review in the light of quality assurance for large PV plants. Renew Sustain Energy Rev 2017;78:780–97. https://doi.org/10.1016/j.rser.2017.04.080.

[77] Chin VJ, Salam Z, Ishaque K. Cell modelling and model parameters estimation techniques for photovoltaic simulator application: A review. Appl Energy 2015;154:500–19. https://doi.org/10.1016/j.apenergy.2015.05.035.

[78] De Soto W, Klein SA, Beckman WA. Improvement and validation of a model for photovoltaic array performance. Sol Energy 2006;80:78–88. https://doi.org/10.1016/j.solener.2005.06.010.

[79] Evans DL, Florschuetz LW. Cost studies on terrestrial photovoltaic power systems with sunlight concentration. Sol Energy 1977;19:255–62. https://doi.org/10.1016/0038-092X(77)90068-8.

[80] Lappalainen K, Valkealahti S. Photovoltaic mismatch losses caused by moving clouds. Sol Energy 2017;158:455–61. https://doi.org/10.1016/j.solener.2017.10.001.

[81] Castellano NN, Gázquez Parra JA, Valls-Guirado J, Manzano-Agugliaro F. Optimal displacement of photovoltaic array's rows using a novel shading model. Appl Energy 2015;144:1–9. https://doi.org/10.1016/j.apenergy.2015.01.060.

[82] Saint-Drenan Y-M, Barbier T. Data-analysis and modelling of the effect of inter-row shading on the power production of photovoltaic plants. Sol Energy 2019;184:127–47. https://doi.org/10.1016/j.solener.2019.03.086.

[83] Mayer MJ, Gróf G. Techno-economic optimization of grid-connected, ground-mounted photovoltaic power plants by genetic algorithm based on a comprehensive mathematical model. Sol Energy 2020;202:210–26. https://doi.org/10.1016/j.solener.2020.03.109.

[84] Chen S, Li P, Brady D, Lehman B. Determining the optimum grid-connected photovoltaic inverter size. Sol Energy 2013;87:96–116. https://doi.org/10.1016/j.solener.2012.09.012.

[85] Driesse A, Jain P, Harrison S. Beyond the curves: Modeling the electrical efficiency of photovoltaic inverters. In: 2008 33rd IEEE Photovolatic Spec. Conf. IEEE; 2008. p. 1–6. https://doi.org/10.1109/PVSC.2008.4922827.

[86] Szintai B, Szűcs M, Randriamampianina R, Kullmann L. Application of the AROME non-hydrostatic model at the hungarian meteorological service: Physical parameterizations and ensemble forecasting. Időjárás 2015;119:241–65.

[87] Tóth Z, Nagy Z, Szintai B. Verification of global radiation fluxes forecasted by numerical weather prediction model AROME for Hungary. Időjárás 2017;121:189–208.

[88] Killinger S, Engerer N, Müller B. QCPV: A quality control algorithm for distributed photovoltaic array power output. Sol Energy 2017;143:120–31. https://doi.org/10.1016/j.solener.2016.12.053.

[89] Murphy AH, Winkler RL. A General Framework for Forecast Verification. Mon Weather Rev 1987;115:1330–8. https://doi.org/10.1175/1520-0493(1987)115<1330:AGFFFV>2.0.CO;2.

[90] Antonanzas J, Perpinan-Lamigueiro O, Urraca R, Antonanzas-Torres F. Influence of electricity market structures on deterministic solar forecasting verification. Sol Energy 2020:1–3. https://doi.org/10.1016/j.solener.2020.04.017.

[91] Yang D, Perez R. Can we gauge forecasts using satellite-derived solar irradiance? J Renew Sustain Energy 2019;11:023704. https://doi.org/10.1063/1.5087588.

[92] Murphy AH. Climatology, persistence, and their linear combination as standards of reference in skill scores. Weather Forecast 1992;7:692–8. https://doi.org/10.1175/1520-0434(1992)007<0692:CPATLC>2.0.CO;2.

[93] Lorenz E, Heinemann D, Kurz C. Local and regional photovoltaic power prediction for large scale grid integration: Assessment of a new algorithm for snow detection. Prog Photovoltaics Res Appl 2012;20:760–9. https://doi.org/10.1002/pip.1224.

[94] Yang D. Standard of reference in operational day-ahead deterministic solar forecasting. J Renew Sustain Energy 2019;11:053702. https://doi.org/10.1063/1.5114985.

[95] Larson DP, Nonnenmacher L, Coimbra CFM. Day-ahead forecasting of solar power output from photovoltaic plants in the American Southwest. Renew Energy 2016;91:11–20. https://doi.org/10.1016/j.renene.2016.01.039.

[96] Hofmann M, Seckmeyer G. Influence of various irradiance models and their combination on simulation results of photovoltaic systems. Energies 2017;10:1495. https://doi.org/10.3390/en10101495.

[97] Gueymard CA. Cloud and albedo enhancement impacts on solar irradiance using high-frequency measurements from thermopile and photodiode radiometers. Part 1: Impacts on global horizontal irradiance. Sol Energy 2017;153:755–65. https://doi.org/10.1016/j.solener.2017.05.004.

[98] Sun X, Bright JM, Gueymard CA, Acord B, Wang P, Engerer NA. Worldwide performance assessment of 75 global clear-sky irradiance models using Principal Component Analysis. Renew Sustain Energy Rev 2019;111:550–70. https://doi.org/10.1016/j.rser.2019.04.006.

[99] Chan AKY, Macabebe EQB. Photovoltaic system performance model for output power forecasting. In: 2019 IEEE PES Asia-Pacific Power Energy Eng. Conf. IEEE; 2019. p. 1–6. https://doi.org/10.1109/APPEEC45492.2019.8994607.

[100] PV Performance Modeling Collaborative n.d. https://pvpmc.sandia.gov/ [accessed July 12, 2020].

[101] Yang D. A guideline to solar forecasting research practice: Reproducible, operational, probabilistic or physically-based, ensemble, and skill (ROPES). J Renew Sustain Energy 2019;11:20. https://doi.org/10.1063/1.5087462.

[102] Kühnert J, Lorenz E, Heinemann D. Satellite-based irradiance and power forecasting for the german energy market. In: Sol. Energy Forecast. Resour. Assess. Elsevier; 2013. p. 267–97. https://doi.org/10.1016/B978-0-12-397177-7.00011-5.

[103] Kim CK, Kim H-G, Kang Y-H, Yun C-Y, Kim SY. Probabilistic prediction of direct normal irradiance derived from global horizontal irradiance over the Korean Peninsula by using Monte-Carlo simulation. Sol Energy 2019;180:63–74. https://doi.org/10.1016/j.solener.2019.01.030.

[104] Quan H, Yang D. Probabilistic solar irradiance transposition models. Renew Sustain Energy Rev 2020;125:109814. https://doi.org/10.1016/j.rser.2020.109814.

[105] Mayer MJ, Szilágyi A, Gróf G. Ecodesign of ground-mounted photovoltaic power plants: Economic and environmental multi-objective optimization. Journal of Cleaner Production 2020;278:123934. https://doi.org/10.1016/j.jclepro.2020.123934.